

Binding and structure of tetramers in the scaling limit

M. R. Hadizadeh^{1,*}, M. T. Yamashita^{1,†}, Lauro Tomio^{1,2,‡}, A. Delfino^{2,§} and T. Frederico^{3,¶}

¹*Instituto de Física Teórica, Universidade Estadual Paulista, 01140-070, São Paulo, SP, Brazil*

²*Instituto de Física, Universidade Federal Fluminense, 24210-346, Niterói, RJ, Brazil*

³*Instituto Tecnológico de Aeronáutica, DCTA, 12228-900, São José dos Campos, SP, Brazil*

(Dated: December 3, 2024)

The momentum-space structure of the Faddeev-Yakubovsky (FY) components of weakly-bound tetramers is investigated at the unitary limit using a renormalized zero-range two-body interaction. The results, obtained by considering a given trimer level with binding energy B_3 , provide further support to a universal scaling function relating the binding energies of two successive tetramer states. The correlated scaling between the tetramer energies comes from the sensitivity of the four-boson system to a short-range four-body scale. Each excited N -th tetramer energy $B_4^{(N)}$ moves as the short-range four-body scale changes, while the trimer properties are kept fixed, with the next excited tetramer $B_4^{(N+1)}$ emerging from the atom-trimer threshold for a universal ratio $B_4^{(N)}/B_3 = B_4^{(N)}/B_4^{(N+1)} \simeq 4.6$, which does not depend on N . We show that both channels of the FY decomposition [atom-trimer (K -type) and dimer-dimer (H -type)] present high momentum tails, which reflect the short-range four-body scale. We also found that the H -channel is favored over K -channel at low momentum when the four-body momentum scale largely overcomes the three-body one.

PACS numbers: 67.85.-d, 21.45.-v, 03.65.Ge, 05.10.Cc, 31.15.-p, 31.15.ac

I. INTRODUCTION

A limit cycle in physics [1] refers to a model independent way to look for a manifestation of a hidden scale, one in which a correlation between physical quantities is geometrically rescaled and replicates itself. Limit cycles are shown to exist even in simple quantum three-boson systems [2–4], manifested for large two-body scattering lengths, as well as for short-ranged interactions. They follow the 1970 Efimov key prediction [5] of geometrically separated weakly-bound three-boson states near the scattering threshold, confirmed by recent experiments in cold-atom traps [6–8]. For a more recent exposition on the experimental status, see Ref. [9]. The addition of one more particle to the quantum three-body system has long challenged this picture [10–13]. Recent theoretical works [14–21] motivated by cold-atom experiments [22–24] have revived this issue. The actual relevance in identifying simple universal relations in few-body binding laws, with the corresponding experimental possibilities, have been discussed by Modugno [25] in a recent perspective article on this matter.

In Ref. [26], we reported a different dimension of this problem by establishing a new universal correlation among the binding energies of two successive tetramer states between two Efimov trimers, through precise numerical calculations within a zero-range interaction at the unitary limit (zero two-body binding). It was

shown that such tetramer states are related to an unsuspected new limit cycle not constrained by Efimov physics or by three-body properties. Tetramers hitting the atom-trimer threshold, leading to resonant recombination losses in this channel, are signatures of a new limit cycle. Furthermore, other four-boson observables close to the unitary limit can exhibit correlations not constrained by the low-energy two- and three-boson properties. Recombination rates, atom-trimer or dimer-dimer scattering lengths, can move near the Feshbach resonance (FR) independently of the two and three-body properties. The appearance of few-body forces in the open channel, due to the coupling with the closed channel, can drive the four-body physics [15]. Indeed, there is a recent experimental evidence, reported by Nakajima et al. [27], of a three-body force acting in the open channel near the FR in a three-component mixture of a ${}^6\text{Li}$ cold gas.

An appropriate way to directly probe the universal properties of a few-boson system at low energy near the unitary limit is to present results in terms of scaling functions correlating pair of observables, within a renormalized zero-range two-body interaction. In this way, no effect can be claimed to be originated from a particular form of the short-range interaction between the particles, as evidenced by the three-body universal scaling function derived in Ref. [2]. As shown in this case, the regularization parameter in the renormalized zero-range approach can be directly associated to a three-boson physical information, in addition to a two-body observable, such as the scattering length. The concept of scaling functions, which is used to evidence universal properties of three-boson systems close to the unitary limit, is extended to four-boson systems in Ref. [26], as well as in the present work. Within such purpose, we study the sensitivity of tetramer properties to a four-boson scale, by using

* hadizade@ift.unesp.br

† yamashita@ift.unesp.br

‡ tomio@ift.unesp.br

§ delfino@if.uff.br

¶ tobias@ita.br

the Faddeev-Yakubovsky (FY) formalism [28, 29] with zero-range two-body interactions. Therefore, independently on the choice of the three-body scale that fixes the trimer properties [15], a four-body regularization parameter (four-body scale) is introduced in the FY formalism. The new short-range scale has indeed effects on four-boson physics, which appears as universal correlations between four-boson low-energy s -wave observables not constrained by the trimer properties. The four-body quantities changes as long as the new scale varies.

Previous conclusions for the nonexistence of a proper four-body scale rely on a strong suppression of the short-range physics, beyond that already accounted for in the three-boson system. Indeed, by estimating the trace of the kernel of the four-body equation in momentum space, Amado and Greenwood [10] showed that there is no infrared divergence, which led them to conclude against the existence of Efimov effect in the case of four or more particles. However, the momentum integrals should also implicitly have an ultraviolet cutoff (the four-body one) to regulate them. Note that according to Weinberg's eigenvalue criterion [30] the divergence of the trace is a necessary condition for an infinite number of bound states. However, in the kernel of the FY equation, this criterion can only be applied when considering the trimer in the ground state. More explicitly, in case of ultraviolet divergence of the four-body kernel, by moving a four-body scale in relation to the three-body one, an infinite number of tetramer states emerges from the threshold, but the number is restricted by the energy interval between trimers (when the reference trimer is an excited one), such that it can be infinite only in case the given trimer is the ground state.

It is also instructive to recall other pioneering four-body calculations that have verified the possibility of Efimov-like behavior in four-body systems, such as the works of Kröger and Perne [11] and Tjon and Naus [13]. Conclusions drawn within the nuclear physics context are obviously limited, in view of the strong nuclear repulsion of the potential core, such that the possible observation of a four-body scale, independent from the three- and two-body ones, is suppressed. It explains why the ${}^4\text{He}$ and the triton binding energies are strongly correlated with a fixed slope, as verified by Tjon [31]. In our understanding of the four-body problem, it is not enough only two parameters, which determines trimer properties, to describe the four-boson system. Our results imply that the correlation between the tetramer and trimer binding energies forms a family of Tjon lines with slopes depending on the new four-boson scale. To exemplify that, we have shown a four-boson universal correlation among the energies of two successive trimers appearing between two consecutive Efimov states [26]. The correlation exhibits a dependence on a new scale not fixed only by the trimer properties. In order to directly address this novel universal behavior, we have performed a number of calculations of tetramer properties within a zero-range model to show how the dependence on the new short-range scale

is evidenced through their structure in momentum space.

The tetramer energies can be presented in a scaling plot where the behavior of a four-body scale can be easily verified in comparison with other relevant few-body scales [26]. The existence of a short-range four-body scale, which is independent of the two- and three-body ones, is expressed in terms of scaling functions or correlation between observables. Once the short-range parameters are eliminated in favor of physical quantities, the renormalized results appear as correlations between the four-body observables with fixed dimer and trimer properties.

In the present work we provide details for the approach that lead us to report [26] a universal correlation between the energies of two successive trimers. As it will be thoroughly presented in the next sections, we establish by our numerical investigations that a new short-range parameter is necessary to fix the properties of the four-boson system in the unitary limit. Our conclusions are supported by precise numerical solutions of the four-boson FY integral equations in momentum space for a zero-range two-body interaction [15], as well as by an analysis of the four-body wave function.

The paper is organized as follows: in Sect. II, we present the FY formalism, within a renormalized zero-range interaction. The relevant scales are introduced in the formalism through a subtractive renormalization approach. In Sect. III, the scaling functions for the binding energies of trimers and trimers are discussed, following Refs. [2] and [26]. Numerical results close to the unitary limit are also reported in this section. In Sect. IV, we present our main results for the structure of universal trimers. We include in this section an extended analysis of the low and high momentum structures of the atom-trimer [(A+T) or K -type] and dimer-dimer [(D+D) or H -type] components of the FY decomposition, to pin down where the manifestation of the short-range four-body scale is more evident. The behavior of the four-body FY components of the wave function is presented in this section. Finally, in Sect. V, we present our conclusions with perspectives in relation to possible experimental observations. Three appendices are supplying further details on our approach: In A and B, we have details on the four-body formalism and total wave function in momentum space. In C, we discuss stability and convergence of our numerical approach, and give some details on the Lanczos-type procedure for solution of the coupled FY equations.

II. FADDEEV-YAKUBOVSKY FORMALISM

The treatment of four-body problems is quite well known in the quantum scattering theory, following the original Faddeev formulation of the three-body systems [28], later on extended to N -particle scattering by Yakubovsky [29]. The actually known Faddeev-Yakubovsky formalism has been considered by several au-

thors in their effort to solve different aspects of four-body systems, in nuclear and atomic physics. In addition to the works on four-body systems already cited in the introduction, we can also mention several other reference works concerning details of the bound-state four-body FY formalism, such as Refs. [32–41] and references therein. Alternatively, in the solution of four-body systems with separable interactions, several authors (exemplified by Refs. [42–45]) have applied the Alt-Grassberger-Sandhas formalism [46], in which the t-matrix components are used instead of the wave-functions.

Here, we describe the FY formalism for bound states of four identical bosons, by considering general separable two-body interactions. Within our approach, the form-factors of the separable potential are conveniently replaced by point-like interactions, within a renormalized zero-range model where the three- and four-body scales are introduced.

A. Bound-state equations and notation

In a four-body (4B) system (with particles i, j, k and l) there are 18 different coordinate systems, each one associated with a specific two-body partition (see Appendices A and B). Basically, by considering the arrangements of the corresponding two- and three-body sub-systems, two different partitions are possible: K -type (A+T), where a single particle is bound to a three-body subsystem; and H -type (D+D), where two dimers are bound. Clearly, as we know from the Faddeev formalism, each three-body subsystem has also three atom-dimer partitions.

We present below the FY formalism with our notation, which is used along the next sections. The bound state of four particles which interact via pairwise forces V_{ij} is given by the Schrödinger equation,

$$|\Psi\rangle = G_0 \sum_{i<j} V_{ij} |\Psi\rangle = \sum_{i<j} |\psi_{ij}\rangle, \quad (1)$$

where $|\psi_{ij}\rangle = G_0 V_{ij} |\Psi\rangle$, $G_0 = (E - H_0)^{-1}$ is the free four-body resolvent and H_0 stands for the free Hamiltonian. The above components satisfy:

$$\begin{aligned} |\psi_{ij}\rangle &= G_0 t_{ij} \sum_{kl \neq ij} |\psi_{kl}\rangle \\ &= G_0 t_{ij} \left(|\psi_{ik}\rangle + |\psi_{il}\rangle + |\psi_{jk}\rangle + |\psi_{jl}\rangle + |\psi_{kl}\rangle \right), \end{aligned} \quad (2)$$

where the two-body transition operator is t_{ij} . The FY decomposition of $|\psi_{ij}\rangle$ reads:

$$\begin{aligned} |K_{ij,k}^l\rangle &= G_0 t_{ij} \left(|\psi_{ik}\rangle + |\psi_{jk}\rangle \right), \\ |K_{ij,l}^k\rangle &= G_0 t_{ij} \left(|\psi_{il}\rangle + |\psi_{jl}\rangle \right), \\ |H_{ij,kl}\rangle &= G_0 t_{ij} |\psi_{kl}\rangle, \end{aligned} \quad (3)$$

where $|K_{ij,k}^l\rangle$ and $|H_{ij,kl}\rangle$ correspond, respectively, to a K -type and H -type partitions. The Faddeev components of the wave function

$$|\psi_{ij}\rangle = |K_{ij,k}^l\rangle + |K_{ij,l}^k\rangle + |H_{ij,kl}\rangle, \quad (4)$$

are reconstructed through FY components.

Every $|\psi_{ij}\rangle$ component contains two K -type and one H -type configurations. Therefore, the total wave function $|\Psi\rangle$ contains twelve different K -type chains and six H -type chains, leading to eighteen independent FY components. By considering identical bosons, the four-body wave function $|\Psi\rangle$ has to be totally symmetric. As a consequence, all twelve K -type components are identical in their functional form with particles permuted. The same is true for the six H -type components. Thus, it is sufficient to consider only two independent FY components corresponding to the K - and H -type partitions, $|K\rangle \equiv |K_{ij,k}^l\rangle$ and $|H\rangle \equiv |H_{ij,kl}\rangle$. The 18 coupled FY equations, for identical bosons, shrink to two coupled homogeneous equations,

$$\begin{aligned} |K_{ij,k}^l\rangle &= G_0 t_{ij} P \left[(1 + P_{kl}) |K_{ij,k}^l\rangle + |H_{ij,kl}\rangle \right], \\ |H_{ij,kl}\rangle &= G_0 t_{ij} \tilde{P} \left[(1 + P_{kl}) |K_{ij,k}^l\rangle + |H_{ij,kl}\rangle \right], \end{aligned} \quad (5)$$

where P_{kl} is the permutation operator for the pair (kl) , with P and \tilde{P} defined by

$$P = (P_{ij} + P_{ik}) P_{jk} \quad \text{and} \quad \tilde{P} = P_{ik} P_{jl}. \quad (6)$$

The symmetry property of $|K\rangle$ under exchange of particles i and j , and $|H\rangle$ under separate exchanges of particles i, j and k, l guarantee that the full wave function,

$$\begin{aligned} |\Psi\rangle &= (1 + P + P_{kl} P + \tilde{P}) \left[(1 + P_{kl}) |K_{ij,k}^l\rangle + |H_{ij,kl}\rangle \right] \\ &= (1 + (1 + P) P_{kl}) (1 + P) |K_{ij,k}^l\rangle \\ &\quad + (1 + P) (1 + \tilde{P}) |H_{ij,kl}\rangle, \end{aligned} \quad (7)$$

is totally symmetric. In order to get insight on how the short-range four-body scale is reflected in the bosonic wave function for a zero-range force, we will analyze the momentum structure of the K and H components. Following this strategy we will be able to map where the new scale is more relevant to build the tetramer wave function. For that purpose, we still simplify the problem using s -wave one-term separable potentials. This class contains, in particular, the contact interaction.

B. One-term separable potential with s -wave projection

In this subsection, to simplify the notation, we use the particle-labels 1, 2, 3 and 4. So, we rewrite Eq.(5) as:

$$\begin{aligned} |K\rangle &= G_0 t_{12} P \left[(1 + P_{34}) |K\rangle + |H\rangle \right], \\ |H\rangle &= G_0 t_{12} \tilde{P} \left[(1 + P_{34}) |K\rangle + |H\rangle \right]. \end{aligned} \quad (8)$$

In order to solve the coupled Eqs. (8) in momentum space one should project these equations into standard sets of Jacobi momenta, corresponding to both, K -type ($|\mathbf{u}_1 \mathbf{u}_2 \mathbf{u}_3\rangle$) and H -type ($|\mathbf{v}_1 \mathbf{v}_2 \mathbf{v}_3\rangle$) partitions, as represented in Fig. 1.

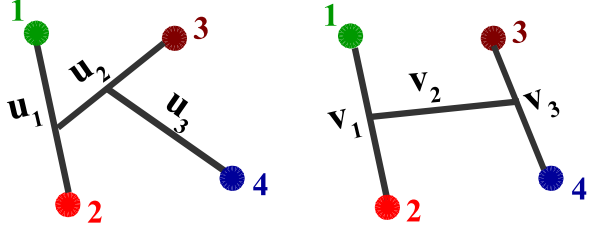


FIG. 1. (Color on-line) Definition of the four-body Jacobi momenta corresponding to the K - and H -type fragmentations.

The standard Jacobi momenta for the 4B system can be defined in terms of the single particle momentum variables $\mathbf{k}_{i=1,2,3,4}$, in two possible configurations (K - and H -type), as shown in Fig. 1:

$$\begin{cases} \mathbf{u}_1 = (1/2)(\mathbf{k}_1 - \mathbf{k}_2), \\ \mathbf{u}_2 = (1/3) [2\mathbf{k}_3 - (\mathbf{k}_1 + \mathbf{k}_2)], \\ \mathbf{u}_3 = (1/4) [3\mathbf{k}_4 - (\mathbf{k}_1 + \mathbf{k}_2 + \mathbf{k}_3)], \end{cases} \quad (9)$$

$$\begin{cases} \mathbf{v}_1 = (1/2)(\mathbf{k}_1 - \mathbf{k}_2), \\ \mathbf{v}_2 = (1/2) [(\mathbf{k}_1 + \mathbf{k}_2) - (\mathbf{k}_3 + \mathbf{k}_4)], \\ \mathbf{v}_3 = (1/2)(\mathbf{k}_3 - \mathbf{k}_4), \end{cases} \quad (10)$$

where we assume identical particles, with mass $m = 1$. Since we are interested in the s -wave channel contribution, we introduce the partial-wave representation of the

four-body projection operators corresponding to each Jacobi momenta set, as

$$|u\rangle \equiv |u_1 u_2 u_3\rangle, \quad |v\rangle \equiv |v_1 v_2 v_3\rangle. \quad (11)$$

Within the s -wave projection, we consider the following completeness relation for both basis sets:

$$\int D^3 U |U\rangle \langle U| = 1, \quad (12)$$

where U indicates each one of u and v sets, with $D^3 U \equiv U_1^2 dU_1 U_2^2 dU_2 U_3^2 dU_3$. Clearly, the projection operators $|u\rangle$ and $|v\rangle$ are adequate to expand $|K\rangle$ and $|H\rangle$ components, respectively. Consequently, the projection of the coupled equations (8) is given by

$$\begin{aligned} \langle u|K\rangle &= \langle u|G_0 t P (1 + P_{34}) |K\rangle + \langle u|G_0 t P |H\rangle, \\ \langle v|H\rangle &= \langle v|G_0 t \tilde{P} (1 + P_{34}) |K\rangle + \langle v|G_0 t \tilde{P} |H\rangle. \end{aligned} \quad (13)$$

In the following, the units are such that $\hbar = 1$ and $m = 1$.

By considering a one-term separable two-body potential operator, $V = \lambda |\chi\rangle \langle \chi|$, the s -wave two-body t -matrix elements can be written, in the K - and H -representations, by

$$\langle U|t|U'\rangle = 4\pi \frac{\delta(U'_2 - U_2) \delta(U'_3 - U_3)}{U_2^2 U_3^2} \chi(U_1) \chi(U'_1) \tau(\epsilon_U), \quad (14)$$

where the corresponding K -type and H -type Jacobi sets, $\{u_1, u_2, u_3\}$ and $\{v_1, v_2, v_3\}$, are represented by $\{U_1, U_2, U_3\}$. In the above, $\tau(\epsilon_U)$ is the reduced scattering amplitude, given by

$$\tau(\mathcal{E}_U) \equiv \left[\frac{1}{\lambda} - \int d^3 p \frac{\chi^2(p)}{\mathcal{E}_U - p^2 + i\delta} \right]^{-1}, \quad (15)$$

where, for the K -type and H -type configurations, respectively, we have,

$$\mathcal{E}_u \equiv E - \frac{3u_2^2}{4} - \frac{2u_3^2}{3}, \quad (16)$$

$$\mathcal{E}_v \equiv E - \frac{v_2^2}{2} - v_3^2. \quad (17)$$

Note that, \mathcal{E}_u and \mathcal{E}_v have different expressions in the K - and H -representations, but are identical when written in terms of the single particle momentum coordinates \mathbf{k}_i .

The final expressions for the FY components in terms of the Jacobi momentum coordinates, derived in the Appendix A through Eqs. (A1-A15), are

$$\begin{aligned}
K(u_1, u_2, u_3) &= 4\pi G_0(u_1, u_2, u_3) \chi(u_1) \tau(\mathcal{E}_u) \int_0^\infty du'_2 u'^2_2 \int_{-1}^1 dx \chi\left(\Pi_1(u_2, u'_2, x)\right) \left[K\left(\Pi_1(u'_2, u_2, x), u'_2, u_3\right) + \frac{1}{2} \int_{-1}^1 dx' \right. \\
&\quad \left. \times \left\{ K\left(\Pi_1(u'_2, u_2, x), \Pi_2(u'_2, u_3, x'), \Pi_3(u'_2, u_3, x')\right) + H\left(\Pi_1(u'_2, u_2, x), \Pi_4(u'_2, u_3, x'), \Pi_5(u'_2, u_3, x')\right) \right\} \right], \\
H(v_1, v_2, v_3) &= 4\pi G_0(v_1, v_2, v_3) \chi(v_1) \tau(\mathcal{E}_v) \int_0^\infty dv'_3 v'^2_3 \chi(v'_3) \left[\int_{-1}^1 dx K\left(v_3, \Pi_6(v_2, v'_3, x), \Pi_7(v_2, v'_3, x)\right) + H\left(v_3, v_2, v'_3\right) \right],
\end{aligned} \tag{18}$$

where the functions $\Pi_{J=1,2,\dots,7}$ are defined by the Eqs. (A5), (A10), (A11), (A13), (A14), (A16) and (A17). Eqs. (18) can be rewritten within new definitions for the

FY components, such as

$$\begin{cases} K(u_1, u_2, u_3) \equiv G_0(u_1, u_2, u_3) \chi(u_1) \mathcal{K}(u_2, u_3), \\ H(v_1, v_2, v_3) \equiv G_0(v_1, v_2, v_3) \chi(v_1) \mathcal{H}(v_2, v_3). \end{cases} \tag{19}$$

Furthermore, by considering a zero-range potential, with $\chi = 1$, the above coupled equations (18) are reduced to the following, where the need of regularization in the momentum integrals is explicit:

$$\begin{aligned}
\mathcal{K}(u_2, u_3) &= 4\pi \tau(\mathcal{E}_u) \int_0^\infty du'_2 u'^2_2 \int_{-1}^1 dx \left[G_0\left(\Pi_1(u'_2, u_2, x), u'_2, u_3\right) \mathcal{K}(u'_2, u_3) \right. \\
&\quad + \frac{1}{2} \int_{-1}^1 dx' \left\{ G_0\left(\Pi_1(u'_2, u_2, x), \Pi_2(u'_2, u_3, x'), \Pi_3(u'_2, u_3, x')\right) \mathcal{K}\left(\Pi_2(u'_2, u_3, x'), \Pi_3(u'_2, u_3, x')\right) \right. \\
&\quad \left. \left. + G_0\left(\Pi_1(u'_2, u_2, x), \Pi_4(u'_2, u_3, x'), \Pi_5(u'_2, u_3, x')\right) \mathcal{H}\left(\Pi_4(u'_2, u_3, x'), \Pi_5(u'_2, u_3, x')\right) \right\} \right], \\
\mathcal{H}(v_2, v_3) &= 4\pi \tau(\mathcal{E}_v) \int_0^\infty dv'_3 v'^2_3 \left[\int_{-1}^1 dx G_0\left(v_3, \Pi_6(v_2, v'_3, x), \Pi_7(v_2, v'_3, x)\right) \right. \\
&\quad \left. \times \mathcal{K}\left(\Pi_6(v_2, v'_3, x), \Pi_7(v_2, v'_3, x)\right) + G_0\left(v_3, v_2, v'_3\right) \mathcal{H}\left(v_2, v'_3\right) \right].
\end{aligned} \tag{20}$$

Following an appropriate renormalization scheme for zero-range interactions, with the regularization parameters directly associated to observables [2], in the regularization of the above coupled equations we introduce the short-range three- and four-body scales, as we are going to discuss in the next subsection.

C. Four-boson zero-range bound-state model

In order to help the understanding of the zero-range model in the four-boson formalism, we shortly review the main steps to deal with two- and three-boson equations, when we have two-body zero-range interactions. The momentum space representation of a zero-range interaction $V(\mathbf{r}) = (2\pi)^3 \lambda \delta(\mathbf{r})$, is characterized by the two-body coupling constant λ and a separable potential with constant form factor ($\langle \mathbf{p} | \chi \rangle = 1$). The matrix element of the two-body transition operator, $\langle p' | t(\mathcal{E}) | p \rangle = \tau(\mathcal{E})$, is

obtained by analytical integration of Eq. (15). The coupling constant λ is fixed by one physical input, e.g., the position of the two-body pole at E_2 :

$$\lambda^{-1} = \int d^3 p \frac{1}{E_2 - p^2} = - \int d^3 p \frac{1}{|E_2| + p^2}. \tag{21}$$

We consider bound or virtual two-body energies, when $E_2 = -|E_2|$. Bound in the case the pole is in the upper part of the complex imaginary axis of the momentum plane ($i\kappa_B$), with corresponding energy in the principal Riemann sheet ($E_2 = -\kappa_B^2$); and virtual when the pole is in the lower part of the complex imaginary axis ($-i\kappa_v$), with the energy in the second Riemann sheet ($E_2 = -\kappa_v^2$). As we are going to consider one case *or* the other, both κ_B and κ_V will be labelled as $\sqrt{B_2}$. Therefore, the corresponding scattering lengths are given by $a = \pm 1/\sqrt{B_2}$ (+ for bound, and - for virtual), with the

renormalized two-body t -matrix given by

$$\tau(\mathcal{E}) = \frac{1/(2\pi^2)}{\sqrt{|E_2|} - \sqrt{-\mathcal{E}}} = \frac{1/(2\pi^2)}{\pm 1/a - \sqrt{|\mathcal{E}|}}. \quad (22)$$

The above procedure is enough to render finite the scattering amplitude, providing the cancelation of the linear divergence of the momentum integral.

1. Subtractive regularization technique

The subtraction technique used to define the two-body scattering amplitude can be generalized to three-boson systems. The need for a new parameter beyond a is demanded by the Thomas collapse [48] of the three particle ground state, when the two-body interaction range r_0 goes to zero. Such collapse is also associated to the Efimov phenomenon by observing that in both the cases $|a|/r_0 \rightarrow \infty$ [49]. The Thomas collapse is avoided at the expense of regularizing the kernel of the three-body equation, which is done by introducing a subtraction at an energy scale $-\mu_3^2$. Together with the two-body scattering length, this procedure determines the low-energy three-boson properties. The regularization of the momentum integration is done by the subtracted form $G_0(E) - G_0(-\mu_3^2)$ in substitution to the free three-body Green's function $G_0(E)$. The regularizing energy parameter μ_3^2 is also called "three-body scale" in view of its direct association to a three-body physical observable (scale) in the renormalization procedure.

By adding a fourth particle to the three-body system, within the same zero-range two-body interaction, another regularization is required in the corresponding formalism, due to new terms in the coupled integral equations, not directly identified with the three-body kernel. This regularization is followed in a similar way as done in the three-boson case, by introducing one more regularizing parameter ("four-body scale"), μ_4^2 , in the FY formalism. This new scaling parameter appears in the integrands associated to the presence of the fourth particle, in order to

allow the complete regularization of all the momentum integrals. Among the 18 FY components, only the first three (i.e. $ijk + l, jki + l$ and $kij + l$) will fully describe the three-body (3B) system (ijk), where the 3B scaling parameter μ_3^2 enters in the subtracted form of the free Green's function. The 4B scaling parameter μ_4^2 enters in the subtracted form of the Green's function that are present in the remaining 15 components. Therefore, in the three components associated to the 3B system, the regularization is done by

$$G_0(E) \longrightarrow G_0^{(3)}(E) \equiv G_0(E) - G_0(-\mu_3^2), \quad (23)$$

with the new scale appearing in the regularization of the other fifteen components:

$$G_0(E) \longrightarrow G_0^{(4)}(E) \equiv G_0(E) - G_0(-\mu_4^2). \quad (24)$$

Summarizing our regularizing approach: The physical scales of the four-body problem are the energies of the dimer, one reference trimer and one reference tetramer. The subtractive procedure adds the regularization parameters μ_3 and μ_4 to the kernel of the FY equations, which are correlated to the physical three- and four-body scales. The dependence on the subtraction points is eliminated in favor of two observables, which in our case are the values of the trimer and tetramer reference energies. The elimination of the dependence on the subtraction point is possible as evidenced by the existence of correlations between four-boson s -wave observables. When presented in terms of dimensionless quantities, the correlation between two consecutive tetramer energies is indeed given by a limit cycle. This correlation, presented in Ref. [26] and further explored in the present work, is in fact consistent with results obtained by other models.

The present four-body regularization strategy keeps fixed the minimal requirement of the three-body properties, while the further freedom is used to introduce the new scale. Therefore, in the regularization procedure of Eqs. (20), by introducing the required three- and four-body regularization parameters as explained above, using (23) and (24), we obtain the corresponding zero-range subtracted FY equations, which are given by:

$$\begin{aligned} \mathcal{K}(u_2, u_3) &= 4\pi \tau(\mathcal{E}_u) \int_0^\infty du'_2 u_2'^2 \int_{-1}^1 dx \left[G_0^{(3)}\left(\Pi_1(u'_2, u_2, x), u'_2, u_3\right) \mathcal{K}(u'_2, u_3) \right. \\ &\quad + \frac{1}{2} \int_{-1}^1 dx' G_0^{(4)}\left(\Pi_1(u'_2, u_2, x), \Pi_2(u'_2, u_3, x'), \Pi_3(u'_2, u_3, x')\right) \mathcal{K}\left(\Pi_2(u'_2, u_3, x'), \Pi_3(u'_2, u_3, x')\right) \\ &\quad \left. + \frac{1}{2} \int_{-1}^1 dx' G_0^{(4)}\left(\Pi_1(u'_2, u_2, x), \Pi_4(u'_2, u_3, x'), \Pi_5(u'_2, u_3, x')\right) \mathcal{H}\left(\Pi_4(u'_2, u_3, x'), \Pi_5(u'_2, u_3, x')\right) \right], \\ \mathcal{H}(v_2, v_3) &= 4\pi \tau(\mathcal{E}_v) \int_0^\infty dv'_3 v_3'^2 \left[G_0^{(4)}\left(v_3, v_2, v'_3\right) \mathcal{H}(v_2, v'_3) \right. \\ &\quad \left. + \int_{-1}^1 dx G_0^{(4)}\left(v_3, \Pi_6(v_2, v'_3, x), \Pi_7(v_2, v'_3, x)\right) \mathcal{K}\left(\Pi_6(v_2, v'_3, x), \Pi_7(v_2, v'_3, x)\right) \right]. \end{aligned} \quad (25)$$

The physical picture behind the regularization leading to (25) can be described as follows. The three-body scale parameterizes the short-range physics in the virtual propagation of the interacting three-boson subsystem within the four-body system. The four-body scale parameterizes the short-range physics beyond the three-body one, explored in the four-boson virtual-state propagation between two different fully interacting three-body or disjoint two-body clusters. It is worthwhile to stress that the first term in the right hand side of the equation for $\mathcal{K}(u_2, u_3)$ is the three-boson bound-state equation, when all the other terms are dropped out. So, it is expected that such term should carry the 3B scale, while one could think that the other terms do not require regularization. However, as shown in [15], still all the other terms need to be regularized, in order to avoid the 4B ground state collapse. Although the same regularizing parameter could also be used in all the terms, the freedom to choose it differently is at our hands, and the constraint of introducing the trimer properties does not require any further assumption, but the given form of the first term in the right-hand side of the equation for $\mathcal{K}(u_2, u_3)$. The physical conditions in coldatom traps that allow us to explore a short-range four-boson independent scale, when approaching the Feshbach resonance, are discussed in Ref. [26].

III. BINDING ENERGIES OF UNIVERSAL TRIMERS AND TETRAMERS

In this section, before considering our numerical results obtained for the FY bound-state equations (25), we provide a brief discussion on scaling functions, starting with the three-boson case (next subsection) and moving to tetramer systems, in subsection III B. After we set up the concept of a scaling function, we will present detailed numerical results for the tetramer binding energies, with a comparison with other recent available calculations. The Lanczos-type procedure for solution of the coupled FY equations is shown in Appendix C, where we also give some details on stability and convergence of our numerical approach.

A. Trimers in the scaling limit

The three-body system is sensitive to the physics at short ranges, which is parameterized by μ_3 . After this scale was recognized [2], it was shown that the change of the three-body scale in respect to the two-body one (e.g., $1/a$) can be clearly revealed by expressing the energies of the Efimov trimers in a single curve, which defines a scaling function $\mathcal{F}_3^{(N)}$. It allows to build the energies of all the sequence of weakly bound trimers. Thus, the

energies of successive trimers are correlated by [2]

$$\sqrt{\frac{B_3^{(N+1)} - \bar{B}_2}{B_3^{(N)}}} \equiv \mathcal{F}_3^{(N)} \left(\pm \sqrt{\frac{B_2}{B_3^{(N)}}} \right), \quad (26)$$

written in terms of dimensionless quantities. For convenience, in (26), we define $\bar{B}_2 \equiv B_2$ for bound two-body systems (plus sign, or $a > 0$), and $\bar{B}_2 \equiv 0$ for virtual states (minus sign, or $a < 0$).

Few cycles are enough to reach a universal function independent on N ; i.e., in the limit $N \rightarrow \infty$ it reaches a renormalization-group invariant limit cycle [1]. At the critical values, $B_3^{(N+1)} = B_2$ (for bound two-body) and $B_3^{(N+1)} = 0$ (for virtual two-body), the scaling function (26) vanishes: $\mathcal{F}_3^{(N)} \left(\pm \sqrt{\frac{B_2}{B_3^{(N)}}} \right) = 0$. In this limit, the solution for a bound two-body system (+ sign) is given by $B_3^{(N)} \simeq 6.925 B_2$; and the solution for a virtual two-body system (- sign) is given by $B_3^{(N)} \simeq 1141 B_2^v$, where B_2^v is the virtual state energy [2, 50]. We observe that the scaling law (26) is one among many possible model independent correlations between three-body observables for short-ranged interactions. We should also point out that range effects can become relevant as $|a|/r_0$ decreases. This is evidenced by the finite-range numerical results from other authors, presented in the scaling plot displayed in Ref. [2]. (On range effects and universal properties of three-body systems, see also Ref. [51].) Therefore, range effects will affect Eq. (26) and the above critical values of $B_3^{(N)}$.

Evidence of Efimov cycles, with a period of 22.7, in the values of the two-body scattering length, a , at the peak of the three-body recombination, were observed in a cold-atom experiment by the Innsbruck group [22], as well as in other recent experiments reported in [9]. These results gave a response to a quite old discussion on the possible realization of the Efimov effect in real physical systems. The Efimov effect was formulated in the nuclear physics context, when considering the solutions of the three-body Faddeev equations in the limit of infinite large two-body scattering length. Since then, the possible existence of Efimov states in nature have been considered in several works, where the most promising one was the calculations done by Cornelius and Glöckle for a system with three atoms of ^4He [52]. The revival of this matter came recently with the advances in cold-atom laboratories, where by using Feshbach resonance techniques it is possible to vary the two-body scattering length from zero to infinite (positive or negative) values.

B. Tetramers in the scaling limit

Following a complete analogy with the three-body case, we now show evidence for the existence of a limit cycle for the binding energies of successive tetramers.

Therefore, by considering a shallow dimer (bound or virtual), we introduce a scaling function for the energies of two successive tetramers between two trimers, as

$$\sqrt{\frac{B_4^{(N+1)} - B_3}{B_4^{(N)}}} \equiv \mathcal{F}_4^{(N)} \left(\sqrt{\frac{B_3}{B_4^{(N)}}}; \pm \sqrt{\frac{B_2}{B_3}} \right). \quad (27)$$

For the present purpose, the calculations are restricted to bound tetramers below the ground trimer, although the results are valid for tetramer attached to different trimers[26].

The scaling function (27) has the dependence on a four-body scale independent of the three- and two-body ones. Due to the flexibility of our model it is transparent how to obtain it. The FY equations (25) are solved for μ_3 fixed while μ_4 is varied. In the unitary limit, the solutions of (25) depends only on the ratio μ_4/μ_3 , with observables given in units of μ_3 . Eliminating the dependence of the tetramer energies on the ratio μ_4/μ_3 by writing the energy of the $(N+1)$ -th state as a function of the energy of the N -th tetramer, the scaling function (27) is constructed, where the dependence on μ_3 is removed in favor of B_3 . As no other scales are present in (25), a scaling function like (27) seems possible. It remains to find whether Eq. (27) is independent on N , which will be discussed in the next subsection.

We observe that, tetramers below a generic trimer are constrained to be between the two successive Efimov trimers. However, below the ground state trimer the tetramer collapses as $\mu_4/\mu_3 \rightarrow \infty$ [15], as it is exemplified in Table I (A), for scale ratios above 200 in the unitary limit.

C. Numerical results close to the unitary limit

The numerical calculations with the renormalized zero-range model requires the definition of the relevant scales. They correspond to the two-, three- and four-body scales given by a^{-1} , μ_3 and μ_4 , and obviously for fixed scattering length and trimer scale one can move μ_4 to investigate its effect on the spectrum of tetramer ground and excited states.

In Table I, we have listed our numerical results for tetramer ground and excited state binding energies. In part (A) the results at unitary limit $B_2 = 0$ are given for different scale ratios from $\mu_4/\mu_3 = 1$ to 400. According to the obtained results for tetramer binding energies, $\mu_4/\mu_3 \simeq 1.6$ is the threshold for the first tetramer excited state, $\mu_4/\mu_3 \simeq 21$ is the threshold for second tetramer excited state and close to $\mu_4/\mu_3 \approx 240$ the third tetramer excited state should appear. At these critical values of scale ratios where $B_4^{(N+1)} = B_3$ with $B_2 = 0$, the scaling function (27) vanishes

$$\mathcal{F}_4^{(N)} \left(\sqrt{\frac{B_3}{B_{4-c}^{(N)}}}; 0 \right) = 0, \quad (28)$$

TABLE I. Binding energies of ground and excited tetramer states, for different four-body scales and for (A) $B_2 = 0$; (B) bound dimer, with $B_2 = 0.02 B_3$; and (C) virtual dimer, with $\sqrt{B_2} = -\sqrt{0.02 B_3}$. In (A), we verify that a third excited tetramer emerges for $\mu_4/\mu_3 \approx 240$. In (B) and (C), for non-zero two-body binding, we have only presented results for the ground and first excited state binding energies.

μ_4/μ_3	$B_4^{(0)}/B_3$	$B_4^{(1)}/B_3 - 1$	$B_4^{(2)}/B_3 - 1$
1	3.10		
1.6	4.70	7.10×10^{-4}	
5	12.5	0.531	
10	24.6	1.44	
21	63.5	3.62	3.20×10^{-4}
40	184	7.65	0.203
50	275	10.8	0.365
70	520	12.9	0.629
100	1.04×10^3	20.5	1.17
200	4.06×10^3	50.8	2.86
300	9.11×10^3	102	4.53
400	1.62×10^4	153	6.28

(A)

μ_4/μ_3	$B_4^{(0)}/B_3$	$B_4^{(1)}/B_3 - 1$
1	2.66	
1.76	4.24	9.8×10^{-4}
5	10.0	0.421
20	45.9	2.77
40	139	6.10
80	506	13.0
200	2.86×10^3	39.5
300	6.00×10^3	69.3
400	9.81×10^3	104

(B)

μ_4/μ_3	$B_4^{(0)}/B_3$	$B_4^{(1)}/B_3 - 1$
1	3.62	
1.7	5.91	0.014
5	15.4	0.658
20	74.8	4.18
40	236	9.46
80	873	20.6
200	5.02×10^3	64.5
300	1.06×10^4	115
400	1.73×10^4	174

(C)

with the solutions approaching $B_{4-c}^{(N)} \simeq 4.6 B_3$, for each cycle, i.e., $N = 0$ and 1, as we have calculated up to three tetramers below the trimer. The limit cycle is approached quite fast, as verified in the case of three-boson [2]. In the critical condition (28) we have one tetramer at the atom-trimer scattering threshold, which allows for a resonant

atom-trimer relaxation in trapped coldatom gases at the Feshbach resonance.

In Table I (B) and (C), we show the numerical results for positive and negative scattering lengths, respectively, with $\sqrt{B_2/B_3} = \pm\sqrt{0.02}$. From these results it is clear that, by comparing with the case of infinite scattering length and for the same scale ratios, the tetramer binding energies for positive and negative scattering lengths have smaller and larger values, respectively. The critical condition for atom-trimer resonant relaxation near the Feshbach resonance, has to be corrected as

$$\mathcal{F}_4^{(N)} \left(\sqrt{\frac{B_3}{B_{4-c}^{(N)}}}; \pm\sqrt{\frac{B_2}{B_3}} \right) = 0, \quad (29)$$

$a = \pm 1/\sqrt{B_2}$ does not vanishes. By performing a linear expansion around $a^{-1} = 0$, from the results given in Table I (B) and (C), one has

$$B_{4-c}^{(N)} \approx 4.6 B_3 \left[1 - 0.8 (a\sqrt{B_3})^{-1} \right]. \quad (30)$$

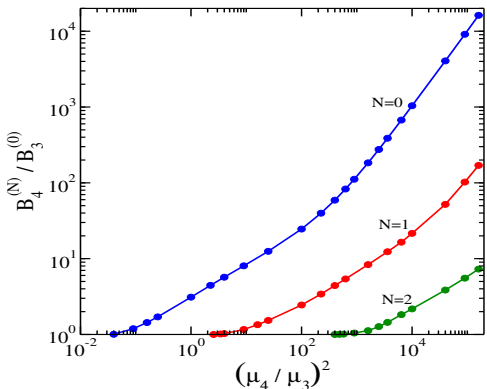


FIG. 2. (Color on-line) The first three tetramer energy levels, in units of the trimer ground state, are shown as functions of $(\mu_4/\mu_3)^2$, where μ_4 and μ_3 are, respectively, the four- and three-body regularizing scaling parameters.

The dependence of the tetramer energies with the ratio μ_4/μ_3 in the unitary limit is presented in Fig. 2 by using results of Table I (A). The collapse of the tetramer states by increasing the short-range four-body momentum scale in respect to the three-body one is seen. As for $1/a = 0$, only two scales define the tetramer state, the four-boson binding increases in respect to the trimer one, by either increasing μ_4 or decreasing μ_3 . The three tetramer states for $N = 0, 1$ and 2 show an increase of the binding energies roughly as μ_4^2 . A similar scaling appears for the trimer binding energy with μ_3^2 . The ratio of B_4/B_3 gives the slope of the Tjon line and it is not a constant as thought before. As a matter of fact it can be considered as a parameter measuring the four-body scale.

In order to compare directly the numerical results for the three- and four-body limit cycle, we present the Fig. 3 with two panels. The three-body Efimov states are shown in the right panel, with the energies given in units of the

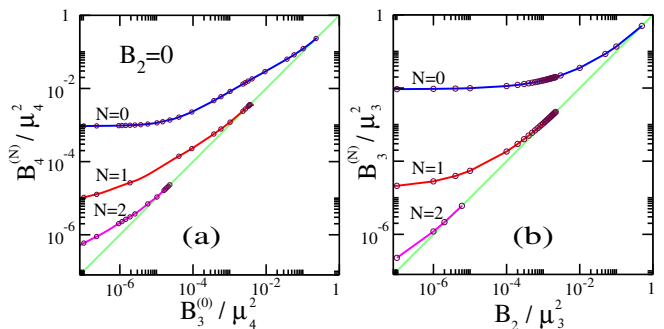


FIG. 3. (Color on-line) In (a) we have the tetramer energy levels $N = 0, 1, 2$, as functions of the trimer ground-state energy for $B_2 = 0$. For comparison, in (b), we have the first Efimov trimer levels as functions of B_2 . The energy units are μ_4^2 , in (a) (where $\mu_3^2 = 1$); and μ_3^2 , in (b). In both cases, the threshold is given by the diagonal line.

trimer scaling parameter μ_3^2 . The corresponding four-body Efimov-like states are given in the left panel, when considering a ground-state trimer in the unitary limit. The dependence of $B_4^{(N)}$ with B_3 are given with the energies in units of the tetramer energy parameter μ_4^2 , for $N = 0, 1$ and 2 (with fixed trimer parameter $\mu_3 = 1$). We illustrate the main qualitative phenomenon of tetramers emerging from the atom plus trimer threshold: by decreasing B_3 , an increasing number of tetramers become bound. A similar phenomenon is shown in the right panel for trimers in terms of a dimer energy, which is the Efimov effect. In our calculations, we first consider tetramers below a trimer in the ground state, such that the tetramer spectrum is not limited from below and can collapse as we increase the four-body scale in relation to the three-body one. In this case, the number of excited tetramer levels can increase with no limit. However, for a given general excited trimer, the applicability of our results are restricted to a region where the trimer energy varies by a factor of about 515 (the Efimov ratio in the unitary limit). Therefore, between two successive trimer states at most three tetramers can be found.

The results for the four-boson binding energies, plotted in Fig. 3(a), exhibit a limit cycle, which expresses the universal behavior of the energies with a moving four-body scale parameter. The curves shown in this figure reduces to a single one, when they are plotted as the correlation between successive tetramer energies, as presented in Fig. 4 for $M = 4$, where we consider the scaling plot in the unitary limit. The scaling function $\mathcal{F}_4^{(N)} \left(\sqrt{B_3/B_4^{(N)}}; 0 \right)$ was built considering up to the third excited state. As in the case of trimer Efimov cycles, the numerical results for tetramers also present a very rapid convergence towards a *four-boson limit cycle*. For comparison, we also present $\mathcal{F}_3^{(N)} \left(\sqrt{B_2/B_3^{(N)}} \right)$, which has the value of $1/22.7$ when B_2 vanishes. The three-body scaling function, identified inside the plot by

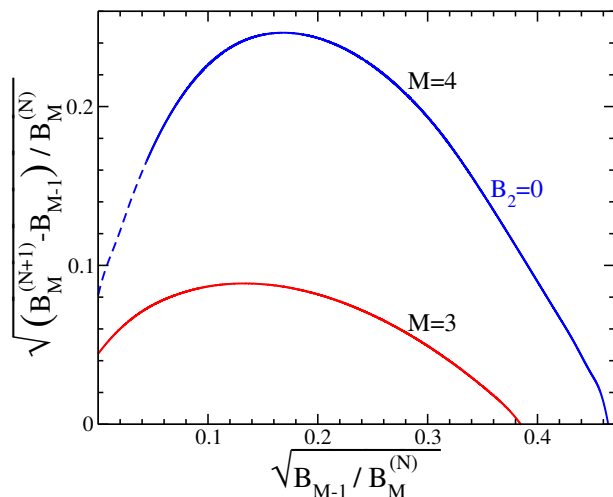


FIG. 4. (Color on-line) The four- and three-body scaling functions are represented, respectively, by $M = 4$ and $M = 3$. The energies are rescaled in terms of B_M^N , where N represents the corresponding energy level in both the cases ($N = 0$ is the ground state). The behavior of excited trimer ($M = 3$) and tetramer ($M = 4$) energies are shown as the corresponding subsystem energy (B_2 or B_3) is varying. In the case of $M = 4$, B_2 is fixed to zero and the dashed part is only reachable by tetramers below the ground-state trimer.

In Fig. 5, to verify the universality of the four-boson scaling function (27) and for comparison, we include results obtained in other recent calculations. In Table II we have listed the available results of other authors, for binding energy ratios of ground and excited tetramers close to the unitary limit. Within those results we should also point out that the ones given in Refs. [17, 19] are for more than one trimer levels. In our results with zero-range interaction, we include not only the exact limit $B_2 = 0$, but also non-zero two-body energies (bound or virtual), as shown in Tables I (A), (B) and (C). The sensibility of the scaling function with variation of the two-body conditions is shown when non-zero two-body energies are used. As it is shown, the exact unitary limit scaling plot is shifted to the right-hand side (left-hand side) when considering non-zero two-body bound (virtual) state energies.

The results of available calculations for tetramer energies plotted in the way we are suggesting put in evidence the effect of the four-body scale. Consistent with our findings, they slide along the universal correlation shown in Fig. 5. The sensitivity of our defined scaling plot, in respect to variations of a two-body observable, as the scattering length or range effects, is also consistent with the results obtained by other authors.

In order to verify the sensitivity of the results (obtained for $B_2 = 0$) with small changes in the dimer energies, we calculate the corresponding scaling functions for a few cases with $B_2 \neq 0$. In the given results, we have

$M = 3$, was derived in Ref. [2], being compared directly with the corresponding four-body scaling function, identified by $M = 4$. The dashed part of the tetramer scaling curve presented in Fig. 4, where $\sqrt{B_3/B_4^{(N)}} < 1/22.7$, is not accessible for the excited tetramer energies belonging to the tetramer spectrum that is obtained for a given *excited* trimer. This restriction implies that a meaningful infinite number of tetramer levels is only possible when considering the trimer in the ground-state level.

Let us consider the unitary limit (when we have the geometrically spaced trimer levels), to resume the global picture suggested by our model. By increasing the tetramer scale in respect to the trimer one, as a new excited tetramer emerges from the threshold, the less excited ones will slide down, moving in direction of the next deeply bound trimer. Actually these tetramers, between two trimers, are resonances decaying to an atom and a trimer. They will dive into the complex plane through the atom-trimer scattering cut with their width increasing as the four-body scale is incremented. This qualitative discussion deserves further investigations from the point of view of the complex analytical structure of the four-body scattering equations. Our picture suggests that, in the unitary limit, at most three tetramer resonances lie between two successive trimers.

three cases for bound two-body systems, where $B_2/B_3 = 0.02, 0.0044, 0.002$, and one case for a virtual two-body state, with $\sqrt{B_2/B_3} = -\sqrt{0.02}$. In Fig. 5, we have also included the Hammer and Platter results for both virtual and real dimer close to unitary limit (See Fig. 2 of Ref. [16]). Despite of the observed difference in the position of both results in our plot, it is remarkable that they both fit nicely in our scaling curve, meaning that the four-boson model of Ref. [16] is sensitive to a four-body scaling parameter, carried out implicitly by the momentum cut-offs used in their calculations.

Although we calculate tetramer energies below the trimer ground state, such that the dashed part of Fig. 4 is also verified, the results for tetramers attached to any other Efimov state, does not change the present conclusions on the existence of a proper four-body scale or its universal manifestation through the scaling function (27), calculated with the zero-range model regularized within our scheme. This fact is evidenced in Fig. 5. Distinct short-ranged interaction models [16, 17, 19–21] show that the energies of successive tetramers linked to the tower of Efimov states scale according to the plot, and thus verifying the universality of the four-boson limit cycle.

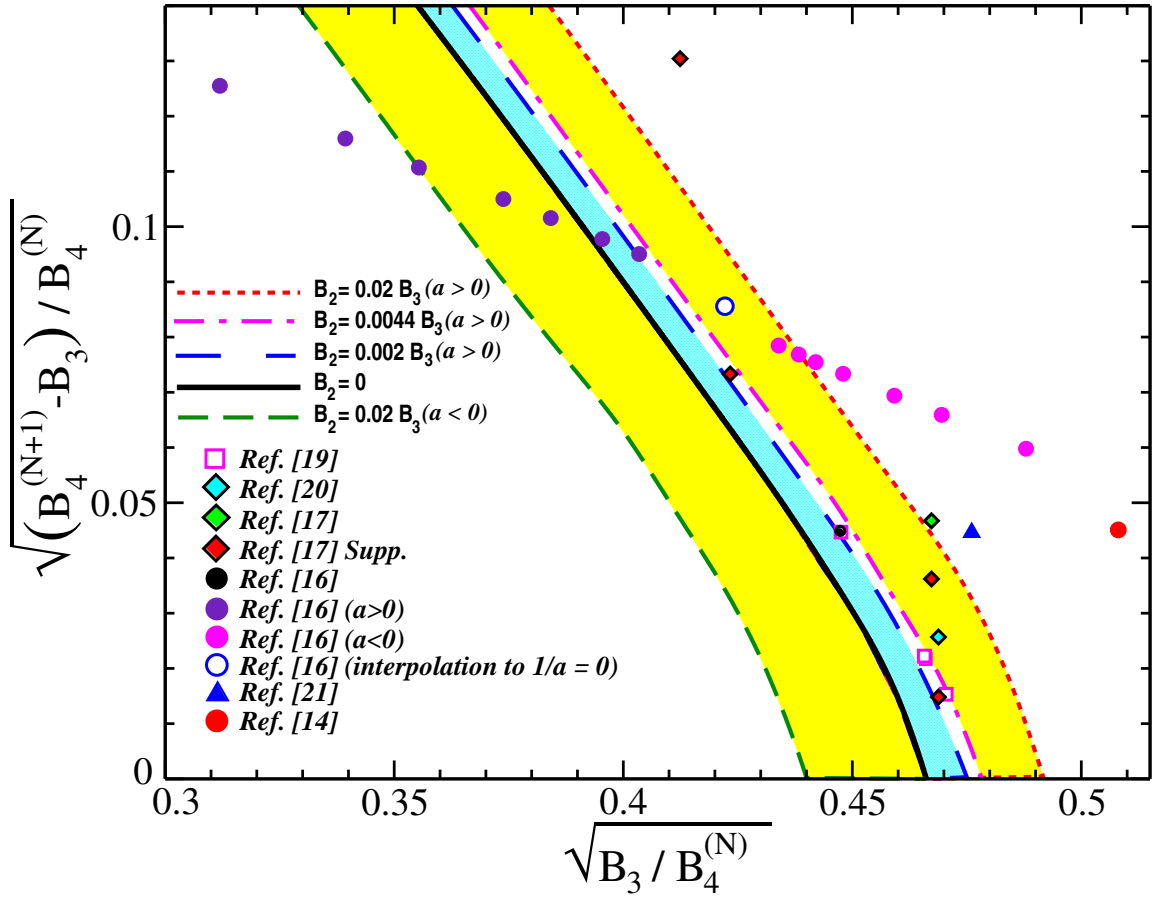


FIG. 5. (Color on-line) Our results for the four-boson scaling function, reported in [26], are displayed in the limited region where more recent results are available. The plots are shown for $B_2 = 0$ (solid-black curve) and in four cases with $B_2 \neq 0$ [three cases with bound dimers, $B_2/B_3 = 0.02, 0.0044, 0.002$, and one case with virtual dimer, $\sqrt{B_2/B_3} = -\sqrt{0.02}$], as indicated inside the frame. In the case of $B_2 = 0$, this figure refers to the right-hand-side corner of Fig. 4 for $M = 4$. The results were explicitly verified numerically for $N = 0$ and $N = 1$, considering the energies $B_4^{N=0,1,2}$, in case $B_2 = 0$; and for $N = 0$ in the other cases where $B_2 \neq 0$. The symbols refer to other model calculations (as indicated) near the unitary limit.

IV. STRUCTURE OF UNIVERSAL TETRAMERS

The effect of the four-body scale on the structure of tetramers at the unitary limit is detailed in this section. We show results for the FY components in momentum space for different scale ratios as well as for momentum probability densities. A close inspection to the reduced FY components, \mathcal{K} and \mathcal{H} , will show how μ_4 manifests through their dependence on the different Jacobi momenta. An analogous study will be presented for the momentum probability densities.

A. Reduced Faddeev-Yakubovsky Components

The reduced FY components $\mathcal{K}(u_2, u_3)$ and $\mathcal{H}(v_2, v_3)$, are shown to spread out up to momentum of the order 1, due to the relevance of the four-body momentum scale μ_4 to regularize the kernel of the set of FY equations

(25) at short distances. Both components have narrow peaks appearing at small momenta, which are even more pronounced for higher scale ratios μ_4/μ_3 and more excited states. They follow a typical tetramer momentum scale ($\sqrt{B_4^{(N)}/\mu_4}$). These features are evident in Figs. 6-8. For a given ratio μ_4/μ_3 , the ground state wave function is more expanded in momentum space in comparison to excited states. The K - and H -channels, and consequently the total wave function for smaller tetramer bindings, should extend to larger distances as compared to the corresponding ones with larger binding.

The peaks at small momentum are due to the nearest trimer pole in the three-boson interacting resolvent, appearing in the K -channel equation (25). This leads to a dominance of \mathcal{K} over \mathcal{H} for small momentum when the tetramer energy approaches B_3 .

In Figs. 6 - 8 we detail the sections of $\mathcal{K}(u_2, u_3)$ and $\mathcal{H}(v_2, v_3)$ with one of the Jacobi momenta being zero for scale ratios of 5, 50 and 200. The interpretation of the

TABLE II. Binding energy ratio of tetramer ground and excited energies to a trimer level, $\left[B_4^{(0)}/B_3, B_4^{(1)}/B_3 - 1\right]$, where the results of Refs.[17, 19] refer to different trimers.

Ref.[53]	Ref.[14]	Ref.[21]	Ref.[16]	Ref.[20]
[4.46,0.06]	[4.075,0.003]	[4.41,0.01]	[5.0,0.01]	[4.55,0.003]

Ref.[17]	Ref.[19]
[4.58, 0.01]	[4.5175, 0.00106]
[5.88, 0.10]	[4.6041, 0.00217]
[4.58, 0.006]	[4.6104, 0.00227]
[5.58, 0.03]	[4.6108, 0.00228]
[4.55, 0.001]	[4.9929, 0.00997]
-	[4.6114,0.00228]

Jacobi momentum in respect to the relevant scales is necessary to proceed in the analysis of these plots. The variable u_2 is the relative momentum of particle 3 in respect to the center of mass of the pair (1,2), which belongs to a trimer configuration (see Fig. 1). Note that in our derivation of the FY equation for the zero range potential, we have chosen to factorize out the dependence of the relative momentum of the pair (1,2) in the definition of the reduced amplitudes, as given by Eq. (19). Naively, by invoking kinematical reasons, it is reasonable to expect that, within the tetramer, the average distance between two bosons is larger than the average distance between the center-of-mass (c.m.) of the virtual pair to the third particle, which is larger than the average distance of the virtual trimer to the fourth particle. The ordering effect comes because the clusters being heavier should have their c.m. closer to the c.m. of the tetramer. This size ordering has a correspondence in respect to the momentum variables. In $\mathcal{K}(u_2, u_3)$, the momentum of the fourth particle in respect to the virtual trimer, u_3 , should explore larger momentum regions than u_2 , which is the relative momentum of the third particle in respect to a pair. An analogous reasoning suggests that the momentum dependence of $\mathcal{H}(v_2, v_3)$ is such that v_2 explores larger momentum regions than v_3 (the relative momentum of two bosons). These qualitative properties are verified in Figs. 6 to 8.

The plots in Fig. 6 show the reduced FY components for the ground, frames (a) and (c), and excited state, frame (b) and (d), for $\mu_4/\mu_3 = 5$. The high momentum tails of $\mathcal{H}(v_2, 0)$ and $\mathcal{K}(0, u_3)$ in respect to $\mathcal{H}(0, v_3)$ and $\mathcal{K}(u_2, 0)$ are visible by comparing the frames (a) and (c) in the case of the ground state, and (b) and (d) for the excited state. By inspecting the pair of frames (a) against (b); and (c) against (d), we also note that all the FY components for the excited state are more concentrated at lower momentum than the corresponding ones for the ground state. Although the binding energy ratio $B_4^{(1)}/B_3$ for the excited state is close to 1, the high momentum

tail bringing the four-body scale is present, giving to this state the possibility to move as μ_4 is changed in respect to μ_3 . These qualitative features are repeated in Figs. 7 and 8, for the scale ratios 50 and 200, respectively, where three tetramer states are possible.

In all the cases we analyzed, the dependence of u_3 in $\mathcal{K}(u_2, u_3)$ and v_2 in $\mathcal{H}(v_2, v_3)$ show that these two variables explore larger momentum regions than u_2 and v_3 , respectively. As we have shown $\mathcal{K}(u_2, 0)$ and $\mathcal{H}(0, v_3)$ have a less prominent tail at large momentum than $\mathcal{K}(0, u_3)$ and $\mathcal{H}(v_2, 0)$. If, for any reason, the high momentum dependence that appears in the K - and H -channel are dropped out, the dependence on the four-body scale will be minimized (may be even completely removed!). Therefore, unreasonable selection of cut-off values in the mapping of momentum variables, which can happen in particular when a fixed cut-off is being used for increasing values of the scale ratios, can lead to convergence in the four-body binding energies rather than collapse. For the discretization of momentum variables one should not only consider large enough cut-off values, consistent with the used four-body scale, but also consider a reasonable number of mesh points in the interval near zero-momentum. Since the iteration of the coupled Eqs. (25) requires a very large number of multi-dimensional interpolations on the Yakubovsky components, we have used Cubic-Hermite Splines to reach high computational accuracy.

From the analysis of Figs. 6 to 8, we conclude that, against the general belief stating that in four-body atomic and nuclear calculations, with model potentials in the FY scheme, the K -channel is always dominant, we show some cases where the H -channel is dominant even at low momentum. This is shown in particular for high scale ratios μ_4/μ_3 .

B. Momentum probability densities

The tetramer wave function $\Psi(u_1, u_2, u_3)$ fully symmetrized is built from Eq. (7) using the definitions (19) of the K and H components in terms of $\mathcal{K}(u_2, u_3)$ and $\mathcal{H}(v_2, v_3)$. In order to simplify our analysis of the wave function, and to obtain an insight on how the momentum is shared among the Jacobi coordinates, we introduce the momentum probability densities $n(u_i)$ as:

$$n(u_i) = u_i^2 \int_0^\infty du_j u_j^2 \int_0^\infty du_k u_k^2 \Psi^2(u_1, u_2, u_3); \quad (31)$$

$$\int_0^\infty du_i n(u_i) = 1,$$

with $(i, j, k) = (1,2,3), (2,3,1)$ and $(3,1,2)$. For reference we use the variables u_i of the K configuration, where u_1 is the relative momentum of a pair, u_2 the relative momentum of the third boson to the C.M. of the pair, and u_3 the relative momentum of the fourth boson to the C.M. of the other three (see fig. 1). As we have discussed in

sect. IV A, the average values of the momentum variables are ordered as $\langle u_1 \rangle < \langle u_2 \rangle < \langle u_3 \rangle$, which is reflected in momentum densities, independent of the degree of excitation of the tetramer.

The momentum probability densities $n(u_1)$, $n(u_2)$ and $n(u_3)$ for scale ratio $\mu_4/\mu_3 = 50$, for ground, first and second excited tetramer states are presented in Fig. 9. In the left panel we show our results for the probability densities in units of μ_4 . Clearly for all three momentum densities, the second excited tetramer leads to a very sharp pick close to zero momentum, whereas for the first excited and ground tetramers the pick is more wide, which is evident as the size is inversely correlated to the tetramer binding energy. For the ground tetramer state the FY components and consequently the 4B total wave function are expanded to higher momentum region and for excited tetramers they are more restricted to zero momentum region. In the right panel of Fig. 9 we present the probability densities in momentum units $\beta_N \equiv \sqrt{B_4^{(N)}}$, for $\mu_4/\mu_3 = 50$. By considering this scaling factor corresponding to the energy of each tetramer state, which from Table I varies two order of magnitude, the densities are amazingly close. The tetramer energy can be considered as the physical scale, which correlates other observables.

One feature of the universal properties of the four-body wave function is presented in Fig. 10, where we have compared the momentum distribution functions $n(u_i)$ of the two shallowest tetramers, for two very different values of μ_4/μ_3 equal to 5 and 50. The functions $n(u_i)$ were rescaled to the same maximum value to make transparent their universal form. The comparison between them clearly confirms a universal dependence of the momentum distributions on the tetramer binding energy. Note that, these quantities are plotted in terms of dimensionless quantities in natural units of the length associated with the tetramer energy.

In Fig. 10 we have shown the renormalized form of the rescaled distribution functions, considering two different scale ratios $\frac{\mu_4}{\mu_3} = 5$ and 50, whereas the distributions are renormalized to the same maximum value. As we have shown the distribution functions have universal shape, independent of the value of scale ratio. We should also add a remark that, in order to simplify the presentation of Fig. 10, we have included only the momentum distribution functions for the two more excited states in case of $\frac{\mu_4}{\mu_3} = 50$, whereas the same universal shape is also obtained for the momentum distribution functions of the ground state (see Fig. 9). The ground state energy ratio is $B_4^{(0)}/B_3 = 275$ (see Table I), which means that $B_4^{(0)}$ is about $2.7\mu_3^2$, while for the two excited states, $B_4^{(1)}$ and $B_4^{(2)}$ is much smaller than μ_3^2 , thus the three-body regularization scale is far more important to the ground state than for the excited states, which approach an universal form for the momentum distribution functions.

C. Tetramer wave function

The calculation of the FY amplitudes K and H , given by Eq. (19) for form factor unity, with the reduced amplitudes \mathcal{K} and \mathcal{H} from the numerical solution of the zero-range FY integral equations (25), allows to build the four-boson wave function fully symmetric by boson exchange. The necessary permutations to reconstruct the 4B wave function from the computed $K(u_1, u_2, u_3)$ and $H(v_1, v_2, v_3)$ are given by introducing permutation operators \mathcal{O} with the corresponding FY amplitudes denoted by $K_{\mathcal{O}}$ and $H_{\mathcal{O}}$ (see Appendix B). Computing $K_{\mathcal{O}}$ and $H_{\mathcal{O}}$ for different \mathcal{O} , the 4B total wave function can be obtained by using Eq. (B1) or (B2).

For our purposes of presenting graphically the total wave function we will show plots for the angle averaged wave function, where the dependence on the relative angles between Jacobi momentum \vec{u}_i ($i = (1, 2, 3)$) is integrated. Our notation is such that we still use $\Psi(u_1, u_2, u_3)$ for the angle averaged wave function. Instead of the usual normalization, we consider

$$\begin{aligned} \langle \Psi | \Psi \rangle &\equiv \int_0^\infty du_1 u_1^2 \int_0^\infty du_2 u_2^2 \int_0^\infty du_3 u_3^2 \Psi^2(u_1, u_2, u_3) \\ &= 1. \end{aligned} \quad (32)$$

In Figs. 11-13 we present our numerical results for the angle averaged total wave function with scale ratio $\mu_4/\mu_3 = 50$, for the ground, first and second excited states. The wave functions are shown as functions of two Jacobi momenta, when the third one is chosen to be zero. As we did before, the magnitudes of Jacobi momenta are re-scaled by the momentum factor $\beta_N \equiv \sqrt{B_4^{(N)}}$ ($N = 0, 1, 2$). In view of the normalization condition (32), this momentum scaling implies in a rescaling of the magnitude of the corresponding total wave function by the factor of $\beta_N^{9/2}$.

The universal form of the 4B wave function is evidenced in Figs. 11-13 by a proper rescaling with the four-body energy. Correspondingly, the contour plots are also presented as functions of two non-vanishing Jacobi momenta, given in units of β_N . Also the momentum density distributions, for two excited states, present a universal form, i.e., independent on the binding energies, when the momentum is measured in units of β_N , as shown in Fig. 9. Note that each of the choices of the vanishing momentum implies in a very long wavelength limit for the fourth particle, indicating the dominance of a three-body cluster configuration within the four-body system. This configuration carries the four-body scale information, as clearly shown by the plots for the wave-function dependence on the two non-vanishing momentum in units of β_N .

V. CONCLUSIONS AND PERSPECTIVES

The momentum-space structure of the FY components of weakly-bound tetramers was thoroughly analyzed at the unitary limit using a renormalized zero-range two-body interaction, with three and four-body scales. Our regularization scheme allows to introduce independently these two scales providing general framework to investigate the universal properties of tetramers, which has extended tails in the classically forbidden region. The step to renormalized results for the observables is found by introducing scaling functions, which are written only in terms of dimensionless physical quantities. These universal scaling functions achieve numerically a limit cycle.

The universal scaling function correlating two successive tetramer energies attached to one trimer comes from the sensitivity of the four-boson system to a short-range four-body scale. Each excited N -th tetramer energy $B_4^{(N)}$ moves as the short-range four-body scale changes while the trimer properties are kept fixed. We suggest that the ratio of B_4/B_3 , which gives the slope of the Tjon line, and it is not a constant as thought before, as a parameter measuring the four-body scale. At the unitary limit, the successive $(N + 1)$ -th tetramer state emerges from the atom plus trimer threshold for a universal ratio $B_4^{(N)}/B_3 = B_4^{(N)}/B_4^{(N+1)} \simeq 4.6$, which does not depend on N . The atom-trimer relaxation resonates when the tetramer hits the scattering threshold.

We also find out that other model results obtained at the unitary limit or close to it [16, 17, 19–21], are quite consistent with our four-boson scaling plot, giving confidence on the universality of our proposed scaling function. As evidenced by our results, the independent behavior of the four-body scale is verified in particular when a universal excited four-boson state pumps out from the atom-trimer threshold as the four-boson parameter is driven to short distances or to the ultraviolet momentum region. In the case that both scales are similar, we confirm that our scaling approach is consistent with the results of other model calculations. We note that the results obtained by other groups appear near the threshold region due to the model assumptions that have been considered, which are much too restrictive when compared to the flexibility of our model and need to be relaxed to allow a wider variation between the four- and three-body properties. The suggested scaling plot offers a model independent way to view the relation between successive tetramer states, which can be verified by experiments exploring two-body scattering lengths very close to the Feshbach resonance, where multi-boson forces are expected to be active [27].

The scaling plot representation exhibiting the dependence on the four-body scale, which is also being confirmed by other models, shows that the model independence is not fortuitous. The reason for that comes from the fact that the wave function of tetramers are largely dominated by configurations where the bosons

are outside the potential range in the classically forbidden region and depend just on two scales at the unitary limit. The sensitivity to the short-range scales appears in both the K - and H -channel of the FY decomposition, which present high momentum tails for any degree of the tetramer excitation. We also found that the H -channel is favored over K -channel at low momentum when the four-body momentum scale largely overcomes the three-body one.

The universal form of the wave function is putted forward at the unitary limit by a scaling plot where the probability momentum densities for different Jacobi momenta are shown in units such that the tetramer binding energy is one. We found that the shapes are independent on the scale ratio and excitation. It only depends on the chosen Jacobi momenta. A simple scaling rule giving the ordering $\langle u_1 \rangle < \langle u_2 \rangle < \langle u_3 \rangle$, where u_1 is the relative momentum of a pair, u_2 is the relative momentum of the third particle to the pair, and u_3 is the relative momentum of the fourth particle in respect to the three-body subsystem.

Our calculations of tetramer binding energies, with corresponding structure of momentum probability density and wave functions, are supplying strong numerical evidences that universal tetramers can arise from the trimer threshold as the four-body scale is moved. These results suggest the possibility of resonant atom-trimer recombination process near the unitary limit, i.e., when $a_{AT} \rightarrow \pm\infty$. It is worth noting that the problem of a new scale in the tetramer properties has a long history, which was never clarified before in the physics community to the extend we are doing now. The four-body scale gives rise to new scalings of tetramer observables which are not determined only by the two and three-body properties. We present detailed and accurate numerical results for the binding and the structure of tetramer states to support our claim, given conveniently within the framework of scaling functions. As a matter of fact, even results obtained near the unitary limit, by authors that are claiming that no four-body scale is necessary, are consistent with the universal scaling plot for the tetramer binding energies.

In our numerical results of four-boson bound states, we first consider the exact unitary limit ($1/a = 0$), and we next consider deviations of this limit to bound ($a > 0$) and virtual ($a < 0$) two-body branches. As shown in Figs. 3-5, universal tetramers can hit the atom-trimer threshold leading to a resonant relaxation in this channel; a crucial phenomenon not considered in other cited recent numerical investigations. In fact, in those analysis, the authors could also have verified the occurrence of tetramer states merging to an atom-trimer threshold, particularly if they had considered the possibility of a four-body independent scaling behavior near a Feshbach resonance. This could be done by including, for example, tunable three or four-body potentials, which would allow an independent change of the three and four-body spectra. The position of the atom-trimer resonance is

not only a function of the atom-atom scattering and the three-body scale, but it also depends on the new four-body scale. Our results do not exclude the resonant dimer-dimer recombination [54] but also add the possibility of a resonant atom-trimer recombination.

Finally, we remark that the four-boson scale can be driven near the Feshbach resonance by induced four-body forces (coming from the one-channel reduction of the atomic interaction) [15, 27]. Therefore, in this case the Efimov ratio percolating the tetramer observables is not assured anymore. Other universal scaling functions can be derived correlating properties of tetramers, in particular the one that correlates the binding energies of tetramers attached to different trimers, and as well as by extending our framework to the scattering region. The possibility that tetramers could be formed and driven in cold-atom laboratories, as have been achieved by radio frequency association techniques applied successfully to measure trimer energies [8], will allow to verify experi-

mentally the universal scaling relations between tetramer properties exhibiting a new scale beyond the trimer one.

ACKNOWLEDGMENTS

We acknowledge partial financial support from the Brazilian agencies Fundação de Amparo à Pesquisa do Estado de São Paulo and Conselho Nacional de Desenvolvimento Científico e Tecnológico.

Appendix A: Momentum space representation of FY equations

In the following we present some details on the FY components in the momentum space representation. By considering the completeness relations, Eq.(12), between the permutation operators, we have

$$\begin{aligned} \langle u|K\rangle &= \int D^3 u' \langle u|G_0 t P|u'\rangle \langle u'|K\rangle + \int D^3 u' D^3 v \langle u|G_0 t P|u'\rangle \langle u'|v\rangle \langle v|H\rangle \\ &+ \int D^3 u' D^3 u'' \langle u|G_0 t P|u'\rangle \langle u'|P_{34}|u''\rangle \langle u''|K\rangle, \end{aligned} \quad (\text{A1})$$

$$\begin{aligned} \langle v|H\rangle &= \int D^3 v' \langle v|G_0 t \tilde{P}|v'\rangle \langle v'|H\rangle + \int D^3 v' D^3 u \langle v|G_0 t \tilde{P}|v'\rangle \langle v'|u\rangle \langle u|K\rangle \\ &+ \int D^3 v' D^3 u D^3 u' \langle v|G_0 t \tilde{P}|v'\rangle \langle v'|u\rangle \langle u|P_{34}|u'\rangle \langle u'|K\rangle. \end{aligned}$$

Therefore, to evaluate the above coupled equations (A1) we need to obtain the following matrix elements:

$$\langle u|G_0 t P|u'\rangle, \quad \langle v|G_0 t \tilde{P}|v'\rangle, \quad (\text{A2})$$

$$\langle u|P_{34}|u'\rangle, \quad \langle u'|v\rangle, \quad \langle v'|u\rangle. \quad (\text{A3})$$

By considering that, in the expressions (A2) we have to insert the two-body matrix elements (14), and that

$$\begin{aligned} \langle u|P|u'\rangle &= \int_{-1}^1 dx \frac{\delta(u_1 - \Pi_1(u_2, u'_2, x))}{u_1^2} \\ &\times \frac{\delta(u'_1 - \Pi_1(u'_2, u_2, x))}{u_1'^2} \frac{\delta(u_3 - u'_3)}{u_3^2}, \end{aligned} \quad (\text{A4})$$

$$\begin{aligned} \Pi_1(u_2, u'_2, x) &\equiv \left| \frac{1}{2} \mathbf{u}_2 + \mathbf{u}'_2 \right| \\ &= \sqrt{\frac{1}{4} u_2^2 + u_2'^2 + u_2 u_2'^2 x}, \end{aligned} \quad (\text{A5})$$

$$\langle v|\tilde{P}|v'\rangle = \frac{\delta(v'_1 - v_3)}{v_1'^2} \frac{\delta(v'_3 - v_1)}{v_3'^2} \frac{\delta(v'_2 - v_2)}{v_2'^2}, \quad (\text{A6})$$

the matrix elements in (A2) are given by the following:

$$\begin{aligned} \langle u|G_0 t P|u'\rangle &= G_0(u_1, u_2, u_3) \int D^3 u'' \langle u|t|u''\rangle \langle u''|P|u'\rangle \\ &= 4\pi G_0(u_1, u_2, u_3) \chi(u_1) \tau(\mathcal{E}_u) \frac{\delta(u'_3 - u_3)}{u_3'^2} \\ &\times \int_{-1}^1 dx \chi\left(\Pi_1(u_2, u'_2, x)\right) \frac{\delta(u'_1 - \Pi_1(u'_2, u_2, x))}{u_1'^2}; \end{aligned} \quad (\text{A7})$$

$$\begin{aligned} \langle v|G_0 t \tilde{P}|v'\rangle &= G_0(v_1, v_2, v_3) \int D^3 v'' \langle v|t|v''\rangle \langle v''|\tilde{P}|v'\rangle, \\ &= 4\pi G_0(v_1, v_2, v_3) \chi(v_1) \chi(v_3) \tau(\mathcal{E}_v) \\ &\times \frac{\delta(v_3 - v'_1)}{v_3^2} \frac{\delta(v_2 - v'_2)}{v_2^2}; \end{aligned} \quad (\text{A8})$$

$$\begin{aligned} \langle u|P_{34}|u' \rangle &= \frac{\delta(u_1 - u'_1)}{u_1'^2} \frac{1}{2} \int_{-1}^1 dx \quad (\text{A9}) \\ &\times \frac{\delta\left(u'_2 - \Pi_2(u_2, u_3, x)\right)}{u_2'^2} \frac{\delta\left(u'_3 - \Pi_3(u_2, u_3, x)\right)}{u_3'^2}, \end{aligned}$$

where

$$\begin{aligned} \Pi_2(u_2, u_3, x) &\equiv \left| \frac{1}{3}\mathbf{u}_2 + \frac{8}{9}\mathbf{u}_3 \right| \quad (\text{A10}) \\ &= \sqrt{\frac{1}{9}u_2^2 + \frac{64}{81}u_3^2 + \frac{16}{27}u_2u_3x}, \end{aligned}$$

$$\begin{aligned} \Pi_3(u_2, u_3, x) &\equiv \left| \mathbf{u}_2 - \frac{1}{3}\mathbf{u}_3 \right| \quad (\text{A11}) \\ &= \sqrt{u_2^2 + \frac{1}{9}u_3^2 - \frac{2}{3}u_2u_3x}; \end{aligned}$$

$$\begin{aligned} \langle u'|v \rangle &= \frac{\delta(v_1 - u'_1)}{v_1'^2} \frac{1}{2} \int_{-1}^1 dx \quad (\text{A12}) \\ &\times \frac{\delta\left(v_3 - \Pi_4(u'_2, u'_3, x)\right)}{v_3'^2} \frac{\delta\left(v_2 - \Pi_5(u'_2, u'_3, x)\right)}{v_2'^2}, \end{aligned}$$

where

$$\begin{aligned} \Pi_4(u_2, u_3, x) &\equiv \left| \frac{1}{2}\mathbf{u}_2 + \frac{2}{3}\mathbf{u}_3 \right| \quad (\text{A13}) \\ &= \sqrt{\frac{1}{4}u_2^2 + \frac{4}{9}u_3^2 + \frac{2}{3}u_2u_3x}, \end{aligned}$$

$$\begin{aligned} \Pi_5(u_2, u_3, x) &\equiv \left| \mathbf{u}_2 - \frac{2}{3}\mathbf{u}_3 \right| \quad (\text{A14}) \\ &= \sqrt{u_2^2 + \frac{4}{9}u_3^2 - \frac{4}{3}u_2u_3x}; \end{aligned}$$

and

$$\begin{aligned} \langle v'|u \rangle &= \frac{\delta(u_1 - v'_1)}{u_1'^2} \frac{1}{2} \int_{-1}^1 dx \quad (\text{A15}) \\ &\times \frac{\delta\left(u_2 - \Pi_6(v'_2, v'_3, x)\right)}{u_2'^2} \frac{\delta\left(u_3 - \Pi_7(v'_2, v'_3, x)\right)}{u_3'^2}, \end{aligned}$$

where

$$\begin{aligned} \Pi_6(v_2, v_3, x) &\equiv \frac{2}{3} \left| \mathbf{v}_2 + \mathbf{v}_3 \right| \quad (\text{A16}) \\ &= \frac{2}{3} \sqrt{v_2^2 + v_3^2 + 2v_2v_3x}, \end{aligned}$$

$$\begin{aligned} \Pi_7(v_2, v_3, x) &\equiv \left| \mathbf{v}_3 - \frac{1}{2}\mathbf{v}_2 \right| \quad (\text{A17}) \\ &= \sqrt{v_3^2 + \frac{1}{4}v_2^2 - v_2v_3x}. \end{aligned}$$

Appendix B: Four-Body Total Wave Functions in Momentum Space

The total four-body wave function, which can be written as

$$\begin{aligned} |\Psi\rangle &= \left(1 + P + P_{34} + PP_{34} + P_{34}P + PP_{34}P\right)|K\rangle \\ &+ \left(1 + P + \tilde{P} + P\tilde{P}\right)|H\rangle, \quad (\text{B1}) \end{aligned}$$

is composed of eighteen FY components, according to the possible arrangements of the four particles ($ijkl$). We have 12 of K -type and 6 of H -type, as follows:

$$\begin{aligned} ijk + l &\rightarrow \begin{cases} ij + k + l &\equiv K_{ij,k}^l \\ jk + i + l &\equiv K_{jk,i}^l = P_{ij} P_{jk} K_{ij,k}^l \\ ki + j + l &\equiv K_{ki,j}^l = P_{ik} P_{jk} K_{ij,k}^l \end{cases} \\ ijl + k &\rightarrow \begin{cases} ij + l + k &\equiv K_{ij,l}^k = P_{kl} K_{ij,k}^l \\ jl + i + k &\equiv K_{jl,i}^k = P_{ij} P_{jl} K_{ij,l}^k \\ li + j + k &\equiv K_{li,j}^k = P_{il} P_{jl} K_{ij,l}^k \end{cases} \\ ikl + j &\rightarrow \begin{cases} ik + l + j &\equiv K_{ik,l}^j = P_{jk} P_{kl} K_{ij,k}^l \\ li + k + j &\equiv K_{li,k}^j = P_{il} P_{lk} K_{ik,l}^j \\ kl + i + j &\equiv K_{kl,i}^j = P_{ik} P_{lk} K_{ik,l}^j \end{cases} \\ jkl + i &\rightarrow \begin{cases} jk + l + i &\equiv K_{jk,l}^i = P_{ij} P_{jk} P_{kl} K_{ij,k}^l \\ lj + k + i &\equiv K_{lj,k}^i = P_{lk} P_{kj} K_{jk,l}^i \\ kl + j + i &\equiv K_{kl,j}^i = P_{lj} P_{kj} K_{jk,l}^i \end{cases} \\ ij + kl &\rightarrow \begin{cases} ij + k + l &\equiv H_{ij,kl} \\ kl + i + j &\equiv H_{kl,ij} = P_{ik} P_{jl} H_{ij,kl} \end{cases} \\ ik + jl &\rightarrow \begin{cases} ik + j + l &\equiv H_{ik,jl} = P_{jk} H_{ij,kl} \\ jl + i + k &\equiv H_{jl,ik} = P_{jk} P_{ik} P_{jl} H_{ij,kl} \end{cases} \\ il + jk &\rightarrow \begin{cases} il + j + k &\equiv H_{il,jk} = P_{ij} P_{jk} P_{ik} P_{jl} H_{ij,kl} \\ jk + i + l &\equiv H_{jk,il} = P_{ij} P_{jk} H_{ij,kl} \end{cases} \end{aligned}$$

In momentum space, we have

$$\begin{aligned} \langle u|\Psi\rangle &= \langle u|1|K\rangle + \langle u|P|K\rangle + \langle u|P_{34}|K\rangle \\ &+ \langle u|PP_{34}|K\rangle + \langle u|P_{34}P|K\rangle + \langle u|PP_{34}P|K\rangle \\ &+ \langle u|1|H\rangle + \langle u|P|H\rangle + \langle u|\tilde{P}|H\rangle + \langle u|P\tilde{P}|H\rangle \\ &\equiv \sum [K_{\mathcal{O}} + H_{\mathcal{O}}]; \quad \mathcal{O} = 1, P, P_{34}, PP_{34}, \dots \quad (\text{B2}) \end{aligned}$$

where

$$\begin{aligned} K_{\mathcal{O}} &\equiv \langle u|\mathcal{O}|K\rangle = \int D^3u' \langle u|\mathcal{O}|u'\rangle \langle u'|K\rangle, \quad (\text{B3}) \\ &= \int D^3u' \langle u|\mathcal{O}|u'\rangle G_0(u'_1, u'_2, u'_3) \chi(u'_1) \mathcal{K}(u'_2, u'_3), \end{aligned}$$

and

$$\begin{aligned} H_{\mathcal{O}} &\equiv \langle u|\mathcal{O}|H\rangle = \int D^3v' \langle u|\mathcal{O}|v'\rangle \langle v'|H\rangle \quad (\text{B4}) \\ &= \int D^3v' \langle u|\mathcal{O}|v'\rangle G_0(v'_1, v'_2, v'_3) \chi(v'_1) \mathcal{H}(v'_2, v'_3). \end{aligned}$$

In the following we present the matrix elements of $K_{\mathcal{O}}$ and $H_{\mathcal{O}}$ explicitly:

$$\begin{aligned} K_1 &\equiv \langle u|1|K \rangle & (B5) \\ &= K(u_1, u_2, u_3) = G_0(u_1, u_2, u_3) \mathcal{K}(u_2, u_3) ; \end{aligned}$$

$$\begin{aligned} K_P &\equiv \langle u|P|K \rangle = \int dx_{12} K\left(\Pi_P^1, \Pi_P^2, u_3\right) & (B6) \\ &= \int dx_{12} G_0\left(\Pi_P^1, \Pi_P^2, u_3\right) \mathcal{K}\left(\Pi_P^2, u_3\right), \end{aligned}$$

where

$$\begin{aligned} \Pi_P^1 &\equiv \Pi_P^1(u_1, u_2, x_{12}) = \left| -\frac{1}{2}\mathbf{u}_1 - \frac{3}{4}\mathbf{u}_2 \right| & (B7) \\ &= \sqrt{\frac{1}{4}u_1^2 + \frac{9}{16}u_2^2 + \frac{3}{4}u_1u_2x_{12}}, \end{aligned}$$

$$\begin{aligned} \Pi_P^2 &\equiv \Pi_P^2(u_1, u_2, x_{12}) = \left| \mathbf{u}_1 - \frac{1}{2}\mathbf{u}_2 \right| & (B8) \\ &= \sqrt{u_1^2 + \frac{1}{4}u_2^2 - u_1u_2x_{12}} ; \end{aligned}$$

$$\begin{aligned} K_{P_{34}} &\equiv \langle u|P_{34}|K \rangle = \frac{1}{2} \int dx_{23} K\left(u_1, \Pi_{P_{34}}^2, \Pi_{P_{34}}^3\right) & (B9) \\ &= \frac{1}{2} \int dx_{23} G_0\left(u_1, \Pi_{P_{34}}^2, \Pi_{P_{34}}^3\right) \mathcal{K}\left(\Pi_{P_{34}}^2, \Pi_{P_{34}}^3\right), \end{aligned}$$

where

$$\begin{aligned} \Pi_{P_{34}}^2 &\equiv \Pi_{P_{34}}^2(u_2, u_3, x_{23}) = \left| \frac{1}{3}\mathbf{u}_2 + \frac{8}{9}\mathbf{u}_3 \right| & (B10) \\ &= \sqrt{\frac{1}{9}u_2^2 + \frac{64}{81}u_3^2 + \frac{16}{27}u_2u_3x_{23}}, \end{aligned}$$

$$\begin{aligned} \Pi_{P_{34}}^3 &\equiv \Pi_{P_{34}}^3(u_2, u_3, x_{23}) = \left| \mathbf{u}_2 - \frac{1}{3}\mathbf{u}_3 \right| & (B11) \\ &= \sqrt{u_2^2 + \frac{1}{9}u_3^2 - \frac{2}{3}u_2u_3x_{23}} ; \end{aligned}$$

$$\begin{aligned} K_{PP_{34}} &\equiv \langle u|PP_{34}|K \rangle & (B12) \\ &= \frac{1}{2} \int dx_{12} \int dx_{12,3} K\left(\Pi_{PP_{34}}^1, \Pi_{PP_{34}}^2, \Pi_{PP_{34}}^3\right) \\ &= \frac{1}{2} \int dx_{12} \int dx_{12,3} G_0\left(\Pi_{PP_{34}}^1, \Pi_{PP_{34}}^2, \Pi_{PP_{34}}^3\right) \\ &\quad \times \mathcal{K}\left(\Pi_{PP_{34}}^2, \Pi_{PP_{34}}^3\right), \end{aligned}$$

where

$$\Pi_{PP_{34}}^1 = \Pi_P^1(u_1, u_2, x_{12}), \quad (B13)$$

$$\Pi_{PP_{34}}^2 = \Pi_{P_{34}}^2\left(\Pi_P^2(u_1, u_2, x_{12}), u_3, x_{12,3}\right), \quad (B14)$$

$$\Pi_{PP_{34}}^3 = \Pi_{P_{34}}^3\left(\Pi_P^2(u_1, u_2, x_{12}), u_3, x_{12,3}\right); \quad (B15)$$

$$\begin{aligned} K_{P_{34}P} &\equiv \langle u|P_{34}P|K \rangle = \frac{1}{2} \int dx_{23} \int dx_{23,1} K\left(\Pi_{P_{34}P}^1, \Pi_{P_{34}P}^2, \Pi_{P_{34}P}^3\right) \\ &= \frac{1}{2} \int dx_{23} \int dx_{23,1} G_0\left(\Pi_{P_{34}P}^1, \Pi_{P_{34}P}^2, \Pi_{P_{34}P}^3\right) \mathcal{K}\left(\Pi_{P_{34}P}^2, \Pi_{P_{34}P}^3\right), \end{aligned} \quad (B16)$$

where

$$\Pi_{P_{34}P}^1 = \Pi_P^1\left(u_1, \Pi_{P_{34}}^2(u_2, u_3, x_{23}), x_{23,1}\right), \quad (B17)$$

$$\Pi_{P_{34}P}^2 = \Pi_P^2\left(u_1, \Pi_{P_{34}}^2(u_2, u_3, x_{23}), x_{23,1}\right), \quad \Pi_{P_{34}P}^3 = \Pi_{P_{34}}^3(u_2, u_3, x_{23}) ;$$

$$\begin{aligned}
K_{PP_{34}P} &\equiv \langle u|PP_{34}P|K \rangle = \frac{1}{2} \int dx_{12} \int dx_{12,3} \int dx_{12;12,3} K \left(\Pi_{PP_{34}P}^1, \Pi_{PP_{34}P}^2, \Pi_{PP_{34}P}^3 \right) \\
&= \frac{1}{2} \int dx_{12} \int dx_{12,3} \int dx_{12;12,3} G_0 \left(\Pi_{PP_{34}P}^1, \Pi_{PP_{34}P}^2, \Pi_{PP_{34}P}^3 \right) \mathcal{K} \left(\Pi_{PP_{34}P}^2, \Pi_{PP_{34}P}^3 \right),
\end{aligned} \tag{B18}$$

where

$$\Pi_{PP_{34}P}^1 = \Pi_P^1 \left(\Pi_P^1(u_1, u_2, x_{12}), \Pi_{P_{34}}^2 \left(\Pi_P^2(u_1, u_2, x_{12}), u_3, x_{12,3} \right), x_{12;12,3} \right), \tag{B19}$$

$$\Pi_{PP_{34}P}^2 = \Pi_P^2 \left(\Pi_P^1(u_1, u_2, x_{12}), \Pi_{P_{34}}^2 \left(\Pi_P^2(u_1, u_2, x_{12}), u_3, x_{12,3} \right), x_{12;12,3} \right), \tag{B20}$$

$$\Pi_{PP_{34}P}^3 = \Pi_{P_{34}}^3 \left(\Pi_P^2(u_1, u_2, x_{12}), u_3, x_{12,3} \right). \tag{B21}$$

For the matrix elements of $H_{\mathcal{O}}$, we need also to evaluate the transformation between the two different representations, i.e., the K - and H -type.

$$\begin{aligned}
H_1 &\equiv \langle u|1|H \rangle = \frac{1}{2} \int dx_{23} H \left(u_1, \Sigma_1^2, \Sigma_1^3 \right) \\
&= \frac{1}{2} \int dx_{23,1} G_0 \left(u_1, \Sigma_1^2, \Sigma_1^3 \right) \mathcal{H} \left(\Sigma_1^2, \Sigma_1^3 \right),
\end{aligned} \tag{B22}$$

where

$$\begin{aligned}
\Sigma_1^2 &\equiv \Sigma_1^2(u_2, u_3, x_{23}) = \left| \mathbf{u}_2 + \frac{2}{3} \mathbf{u}_3 \right| \\
&= \sqrt{u_2^2 + \frac{4}{9} u_3^2 + \frac{4}{3} u_2 u_3 x_{23}}, \\
\Sigma_1^3 &\equiv \Sigma_1^3(u_2, u_3, x_{23}) = \left| \frac{1}{2} \mathbf{u}_2 - \frac{2}{3} \mathbf{u}_3 \right| \\
&= \sqrt{\frac{1}{4} u_2^2 + \frac{4}{9} u_3^2 - \frac{2}{3} u_2 u_3 x_{23}};
\end{aligned} \tag{B23}$$

$$\begin{aligned}
H_P &\equiv \langle u|P|H \rangle \\
&= \frac{1}{2} \int dx_{12} \int dx_{12,3} H \left(\Sigma_P^1, \Sigma_P^2, \Sigma_P^3 \right) \\
&= \frac{1}{2} \int dx_{12} \int dx_{12,3} G_0 \left(\Sigma_P^1, \Sigma_P^2, \Sigma_P^3 \right) \mathcal{H} \left(\Sigma_P^2, \Sigma_P^3 \right),
\end{aligned} \tag{B24}$$

where

$$\Sigma_P^1 = \Pi_P^1(u_1, u_2, x_{12}), \tag{B25}$$

$$\Sigma_P^2 = \Sigma_1^2 \left(\Pi_P^2(u_1, u_2, x_{12}), u_3, x_{12,3} \right), \tag{B26}$$

$$\Sigma_P^3 = \Sigma_1^3 \left(\Pi_P^2(u_1, u_2, x_{12}), u_3, x_{12,3} \right); \tag{B27}$$

$$\begin{aligned}
H_{\tilde{P}} &\equiv \langle u|\tilde{P}|H \rangle = \frac{1}{2} \int dx_{23} H \left(\Sigma_{\tilde{P}}^1, \Sigma_{\tilde{P}}^2, u_1 \right) \\
&= \frac{1}{2} \int dx_{23} G_0 \left(\Sigma_{\tilde{P}}^1, \Sigma_{\tilde{P}}^2, u_1 \right) \mathcal{H} \left(\Sigma_{\tilde{P}}^2, u_1 \right),
\end{aligned} \tag{B28}$$

where

$$\Sigma_{\tilde{P}}^1 = \Sigma_1^3(u_2, u_3, x_{23}), \tag{B29}$$

$$\Sigma_{\tilde{P}}^2 = \Sigma_1^2(u_2, u_3, x_{23}); \tag{B30}$$

$$H_{P\tilde{P}} \equiv \langle u|P\tilde{P}|H \rangle \tag{B31}$$

$$\begin{aligned}
&= \frac{1}{2} \int dx_{12} \int dx_{12,3} H \left(\Sigma_{P\tilde{P}}^1, \Sigma_{P\tilde{P}}^2, \Sigma_{P\tilde{P}}^3 \right) \\
&= \frac{1}{2} \int dx_{12} \int dx_{12,3} G_0 \left(\Sigma_{P\tilde{P}}^1, \Sigma_{P\tilde{P}}^2, \Sigma_{P\tilde{P}}^3 \right) \\
&\quad \times \mathcal{H} \left(\Sigma_{P\tilde{P}}^2, \Sigma_{P\tilde{P}}^3 \right),
\end{aligned}$$

where

$$\Sigma_{P\tilde{P}}^1 = \Sigma_1^3 \left(\Pi_P^2(u_1, u_2, x_{12}), u_3, x_{12,3} \right), \tag{B32}$$

$$\Sigma_{P\tilde{P}}^2 = \Sigma_1^2 \left(\Pi_P^2(u_1, u_2, x_{12}), u_3, x_{12,3} \right), \tag{B33}$$

$$\Sigma_{P\tilde{P}}^3 = \Pi_P^1(u_1, u_2, x_{12}). \tag{B34}$$

Appendix C: On the numerical approach

The final set of homogeneous coupled integral equations in momentum space, after discretization, defines a huge matrix eigenvalue equation, which is solved by iteration within a Lanczos-like method. This method is quite efficient in solving few-body systems. For continuous momentum and angle variables discretization we have used Gaussian-quadrature grid points with hyperbolic and linear mappings, respectively. After considering a convenient mesh distribution to have optimal numerical stability, the number of grid points found necessary in mapping the momentum variable was set up to 140. That was achieved by studying the concentration of the points in the different relevant regions of momentum

integration. For more details on the general numerical techniques that we are considering, see also Ref. [55].

Next, we also address problems concerning to the accuracy and precision of the results in the unitary limit.

1. Numerical convergence

The numerical convergence of our results is exemplified with one case, where stability is more difficult to achieve. As this happens in the excited states of large scale ratios, we choose the case of $\mu_4/\mu_3 = 300$, in which we can verify the existence of up to four tetramers. The number of points and, particularly, their distribution, is quite critical for the accuracy of the excited-state energies and corresponding FY reduced amplitudes. In our systematic study to construct the limit cycle shown in Fig. 5, we are satisfied to achieve $\sim 1\%$ of deviation from the converged results. To be clear, we choose to present in Fig. 14 the convergence in respect to the mesh number of points, for the first and second excited states.

As the corresponding FY components become quite concentrated at the momentum origin, in this case the momentum space discretization u_i is derived from the quadrature Gaussian mesh distribution $x_i \equiv \{-1, +1\}$ by the following hyperbolic mapping:

$$u_i = \frac{1 + x_i}{c_1(1 - x_i) + c_2 x_i}, \quad (\text{C1})$$

with $c_1 \equiv \mu_4/\mu_3$ and $c_2 = 0.4$. In general, we observe that for all the cases with smaller scaling ratios, or for excited states that are not too close to the continuum threshold, i.e., about to be unbound, 140 points are enough to achieve less than 1% of inaccuracy, within an appropriate mesh distribution.

2. Iterative Lanczos-type diagonalization algorithm for solution of the coupled FY equations

The coupled FY integral equations (25) can be schematically represented as an eigenvalue problem:

$$\mathbb{k}(E).\psi = \lambda(E).\psi \quad (\text{C2})$$

where the kernel of integral equations $\mathbb{k}(E)$ is energy dependent, $\lambda(E)$ and ψ are its eigenvalue and eigenvector, correspondingly. The vector ψ is composed of FY components as $\psi = \begin{pmatrix} \mathcal{K} \\ \mathcal{H} \end{pmatrix}$. The binding energy of four-body bound state can be obtained when one of the eigenvalues obtained from the solution of Eq. (C2) for an input energy becomes one ($\lambda(E) = 1$). To this aim one should solve the eigenvalue equation (C2) for a set of input energies.

After discretization of continuous momentum and angle variables, the kernel of the eigenvalue equation turns into a huge matrix with dimensionality of $120 \times 120 \times 120 \times 40 \times 40 \sim 10^9$, where we have used 120 mesh points for Jacobi momentum variables (with a hyperbolic

mapping) and 40 mesh points for angle variables (with a linear mapping). Considering that, exact solutions of huge matrices by diagonalization are not so efficient, we avoid such procedure by using a Lanczos-type technique, which is based on iteration. In this way, one can obtain the eigenvalues and eigenvectors of a huge matrix, from input energies [56]. In the following, we describe some details of this technique.

The iteration procedure is performed with a properly starting vector $\psi_0 = \begin{pmatrix} \mathcal{K}_0 \\ \mathcal{H}_0 \end{pmatrix}$, chosen as Gaussian functions for both \mathcal{K} and \mathcal{H} components. After N iterations, one obtains the set of vectors $\{\psi_i\} = \psi_1, \psi_2, \dots, \psi_N$ where

$$\psi_i = \mathbb{k}(E).\psi_{i-1} \quad ; i = 1, 2, \dots, N \quad (\text{C3})$$

In the iterative diagonalization approach, an orthonormal basis $\{\bar{\psi}_i\}$ can be built up by following a recursive procedure and by using the original vector set $\{\psi_i\}$, where

$$\bar{\psi}_i = c_i \left\{ \psi_i - \sum_{j=1}^{i-1} (\bar{\psi}_j.\psi_i) \bar{\psi}_j \right\} \quad (i = 1, 2, \dots, N). \quad (\text{C4})$$

In the above, c_i are normalization factors which can be obtained by orthogonalization of orthonormal basis states $\bar{\psi}_i.\bar{\psi}_j = \delta_{ij}$. By introducing a matrix D , obtained from the FY components as

$$\begin{aligned} D_{ij} &= \psi_i.\psi_j = \begin{pmatrix} \mathcal{K}_i & \mathcal{H}_i \end{pmatrix} \cdot \begin{pmatrix} \mathcal{K}_j \\ \mathcal{H}_j \end{pmatrix} \\ &= \mathcal{K}_i.\mathcal{K}_j + \mathcal{H}_i.\mathcal{H}_j = D_{ij}^K + D_{ij}^H, \end{aligned} \quad (\text{C5})$$

where

$$\begin{aligned} D_{ij}^K &= \mathcal{K}_i.\mathcal{K}_j = \int du_2 u_2^2 \int du_3 u_3^2 \mathcal{K}_i(u_2, u_3) \mathcal{K}_j(u_2, u_3), \\ D_{ij}^H &= \mathcal{H}_i.\mathcal{H}_j = \int dv_2 v_2^2 \int dv_3 v_3^2 \mathcal{H}_i(v_2, v_3) \mathcal{H}_j(v_2, v_3), \end{aligned} \quad (\text{C6})$$

the normalization factors c_i can be obtained as:

$$c_i = \frac{1}{\sqrt{D_{ii} - \sum_{j=1}^{i-1} N_{ij}^2}}. \quad (\text{C7})$$

The matrix elements N_{ij} are projection of vectors ψ_i on $\bar{\psi}_j$. i.e. $N_{ij} = \psi_i.\bar{\psi}_j$,

$$N_{ij} = c_j \left\{ D_{ij} - \sum_{k=1}^{j-1} N_{ik}.N_{jk} \right\}. \quad (\text{C8})$$

By expanding the original vector ψ , in Eq. (C2), in terms of constructed orthonormal vectors:

$$\psi = \sum_{i=1}^{N-1} g_i \bar{\psi}_i \quad (\text{C9})$$

and projecting the eigenvalue equation onto $\bar{\psi}_j$, the huge dimension of the eigenvalue problem will be reduced to a problem of much smaller dimension $N - 1$:

$$\sum_{i=1}^{N-1} M_{ij} g_i = \lambda g_j \quad (\text{C10})$$

where

$$M_{ij} \equiv \bar{\psi}_i \cdot \mathbb{k} \cdot \bar{\psi}_j \quad (\text{C11})$$

By defining a_{ij} and b_{ij} as coefficients of linear expansion of original vectors in terms of orthonormal vectors and reversely,

$$\psi_i = \sum_{j=1}^i a_{ij} \bar{\psi}_j, \quad \bar{\psi}_i = \sum_{j=1}^i b_{ij} \psi_j, \quad (\text{C12})$$

the matrix elements of M can be obtained as:

$$M_{ij} = \sum_{k=1}^i b_{ik} a_{k+1j} \quad 1 \leq i, j < N \quad (\text{C13})$$

where

$$a_{ij} = \begin{cases} N_{ij} & j < i \\ \frac{1}{c_i} & j = i \end{cases} \quad (\text{C14})$$

$$(\text{C15})$$

$$b_{ij} = \begin{cases} c_j (-\sum_{k=j+1}^i b_{ik} a_{kj}) & j < i \\ \frac{1}{c_i} & j = i \end{cases} \quad (\text{C16})$$

The reduced eigenvalue problem, Eq. (C13), can be solved easily by diagonalization of the matrix M . For a given input energy, one can obtain a set of eigenvalues and their corresponding eigenvectors. In order to obtain the physical binding energy, one should look for an eigenvalue $\lambda = 1$ in the obtained eigenvalue spectrum. Clearly, the eigenvector corresponding to this eigenvalue gives the coefficients g_i . Therefore, by using the Eq. (C9), one can obtain the physical eigenvector or the FY components.

-
- [1] K. G. Wilson, Phys. Rev. D **3**, 1818 (1971).
[2] T. Frederico, L. Tomio, A. Delfino, and A. E. A. Amorim, Phys. Rev. A **60**, R9 (1999).
[3] P. F. Bedaque, H.-W. Hammer, and U. van Kolck, Phys. Rev. Lett. **82**, 463 (1999).
[4] R. F. Mohr, R. J. Furnstahl, H.-W. Hammer, R. J. Perry, and K. G. Wilson, Ann. Phys. **321**, 225 (2006).
[5] V. Efimov, Phys. Lett. B **33**, 563 (1970); V. Efimov, Sov. J. Nucl. Phys. **12**, 589 (1971).
[6] T. Kraemer *et al.*, Nature **440**, 315 (2006).
[7] G. Barontini *et al.*, Phys. Rev. Lett. **103**, 043201 (2009).
[8] T. Lompe *et al.*, Science **330**, 940 (2010).
[9] F. Ferlaino and R. Grimm, Physics **3**, 9 (2010).
[10] R. D. Amado and F. C. Greenwood, Phys. Rev. D **7**, 2517 (1973).
[11] H. Kröger and R. Perne, Phys. Rev. C **22**, 21 (1980).
[12] S. K. Adhikari and A. C. Fonseca, Phys. Rev. D **24**, 416 (1981).
[13] H. W. L. Naus and J. A. Tjon, Few-Body Systems **2**, 121 (1987).
[14] L. Platter, H. W. Hammer, and Ulf-G. Meissner, Phys. Rev. A **70**, 52101 (2004).
[15] M. T. Yamashita, L. Tomio, A. Delfino, and T. Frederico, Europhys. Lett. **75**, 555 (2006).
[16] H.-W. Hammer and L. Platter, Eur. Phys. J. A **32**, 113 (2007).
[17] J. von Stecher, J. P. D’Incao, and C. H. Greene, Nature Physics **5**, 417 (2009).
[18] Y. Wang and B. D. Esry, Phys. Rev. Lett. **102**, 133201 (2009).
[19] A. Deltuva, arXiv:1009.1295v1 [physics.atm-clus]; Phys. Rev. A **82**, 040701(R) (2010).
[20] J. von Stecher, J. Phys. B: At. Mol. Opt. Phys. **43**, 101002 (2010).
[21] R. Lazauskas and J. Carbonell, Phys. Rev. A **73**, 062717 (2006).
[22] F. Ferlaino *et al.*, Phys. Rev. Lett. **102**, 140401 (2009).
[23] M. Zaccanti *et al.*, Nature Phys. **5**, 586 (2009).
[24] S. Pollack *et al.*, Science **326**, 1683 (2009), and www.sciencemag.org/cgi/content/full/1182840/DC1 for Supporting Online Material.
[25] G. Modugno, Science **326**, 1640 (2009).
[26] M. R. Hadizadeh, M. T. Yamashita, L. Tomio, A. Delfino, and T. Frederico, Phys. Rev. Lett. **107**, 135304 (2011).
[27] S. Nakajima, M. Horikoshi, T. Mukaiyama, P. Naidon, and M. Ueda, Phys. Rev. Lett. **105**, 023201 (2010); **106**, 143201 (2011).
[28] L.D. Faddeev, Zh. Eksp. Teor. Fiz. **39**, 1459 (1960) [Sov. Phys. JETP **12**, 1014-1019 (1961)].
[29] O.A. Yakubovsky, Yad. Fiz. **5**, 1312 (1967) [Sov. J. Nucl. Phys. **5**, 937 (1967)].
[30] S. Weinberg, Phys. Rev. **131**, 440 (1963).
[31] J. A. Tjon, Phys. Lett. B **56**, 217 (1975).
[32] T. Sasakawa, Phys. Rev. C **13**, 1801 (1976).
[33] B. F. Gibson and D. R. Lehman, Phys. Rev. C **14**, 685 (1976); Phys. Rev. C **15**, 2257 (1977).
[34] S. P. Merkuriev, S. L. Yakovlev, and C. Gignoux, Nucl. Phys. A **431**, 125 (1984);
[35] N. W. Schellingerhout, J. J. Schut, and L. P. Kok, Phys. Rev. C **46**, 1192 (1992).
[36] H. Kamada and W. Glöckle, Phys. Lett. B **292**, 1 (1992); H. Kamada *et al.*, Phys. Rev. C **64**, 044001 (2001).
[37] A. L. Zubarev and V. B. Mandelzweig, Phys. Rev. C **52**, 509 (1995).
[38] I. N. Filikhin, S. L. Yakovlev, V. A. Roudnev, and B. Vlahovic, J. Phys. A: At. Mol. Opt. Phys. **35**, 501 (2002).
[39] R. Lazauskas and J. Carbonell, Few-Body Syst. **34**, 105 (2004).
[40] S. Bayegan and M. R. Hadizadeh, W. Glöckle, Prog. Theor. Phys. **120**, 887 (2008)
[41] M. R. Hadizadeh, L. Tomio, and S. Bayegan, Phys. Rev. C **83**, 054004 (2011).

- [42] R. Perne and W. Sandhas, Phys. Rev. Lett. **39**, 788 (1977).
- [43] S. A. Sofianos, H. Fiedeldey, H. Haberzettl, and W. Sandhas, Phys. Rev. C **26**, 228 (1982).
- [44] S. Nakaichi-Maeda and T. K. Lim, Phys. Rev. A **28**, 692 (1983).
- [45] A. C. Fonseca, Phys. Rev. C **30**, 35 (1984).
- [46] E. O. Alt, P. Grassberger and W. Sandhas, Phys. Rev. C **1**, 85 (1970).
- [47] T. Frederico, L. Tomio, A. Delfino, M.R. Hadizadeh, and M.T. Yamashita, Few-Body Syst. (2011) [DOI 10.1007/s00601-011-0236-7].
- [48] L. H. Thomas, Phys. Rev. **47**, 903 (1935).
- [49] S. K. Adhikari, A. Delfino, T. Frederico, I. D. Goldman, and L. Tomio, Phys. Rev. A **37**, 3666 (1988).
- [50] L. Tomio, M.T. Yamashita, T. Frederico, and F. Bringas, Laser Physics **21**, 1464 (2011).
- [51] M. Thøgersen, D. V. Fedorov, and A. S. Jensen, Phys. Rev. A **78**, 020501(R) (2008).
- [52] Th. Cornelius and W. Glöckle, J. Chem. Phys. **85**, 1 (1986).
- [53] D. Blume and C. Greene, J. Chem. Phys. **112**, 8053 (2000).
- [54] J. P. D’Incao, J. von Stecher, and C. H. Greene, Phys. Rev. Lett. **103**, 033004 (2009).
- [55] M. R. Hadizadeh and S. Bayegan, Few Body Syst. **40**, 171 (2007).
- [56] A. Stadler, W. Glöckle, and P. U. Sauer, Phys. Rev. C **44**, 2319 (1991).

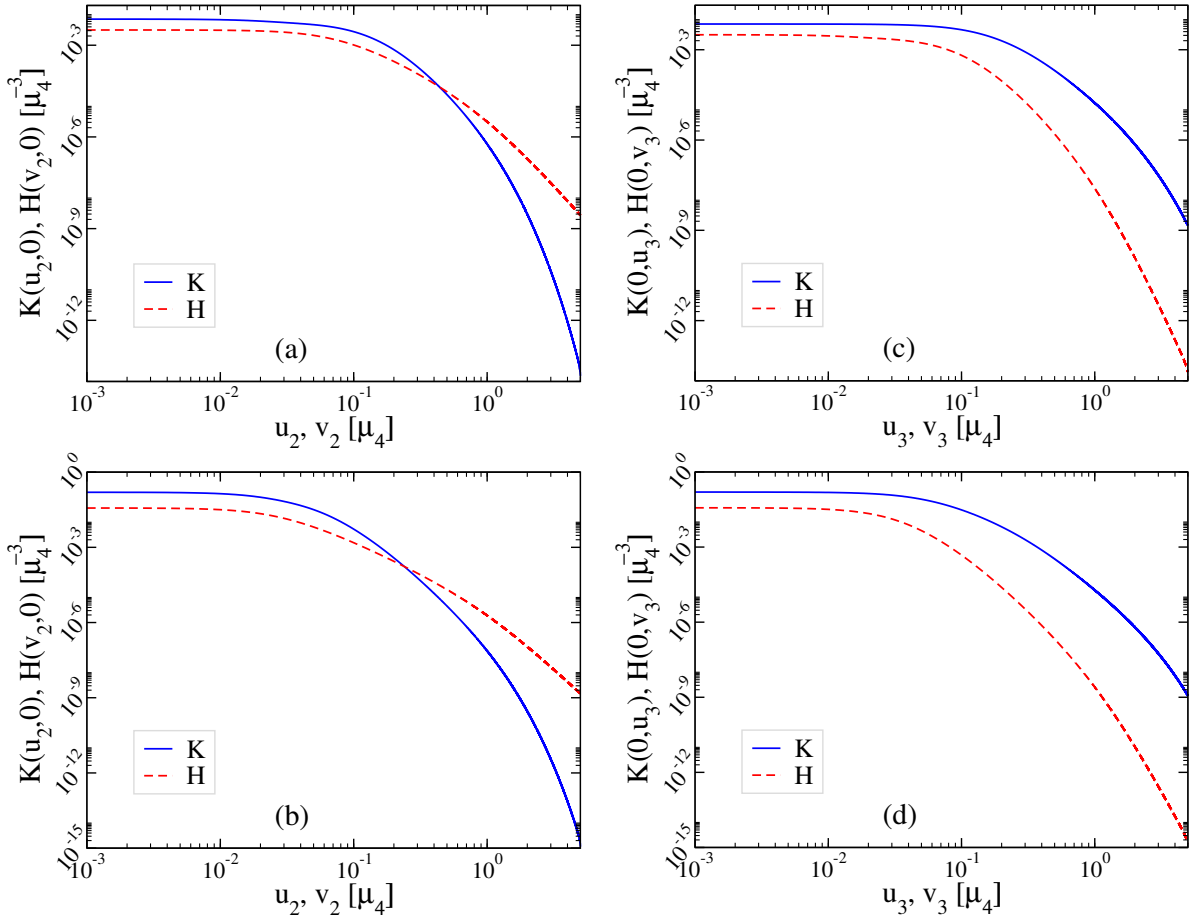


FIG. 6. (Color on-line) The Yakubovsky components \mathcal{K} and \mathcal{H} , as functions of the Jacobi momenta for scale ratio $\mu_4/\mu_3 = 5$, when only one four-body excited state exists. In Figs. (a) and (b) the components are shown as a function of u_2, v_2 where $u_3, v_3 = 0$ and in Figs. (c) and (d) are shown as function of u_3, v_3 where $u_2, v_2 = 0$. In (a) and (c) we have results for the ground-state level; and in (b) and (d) for the first excited-state level. The normalization is such that $\int_0^\infty du_2 u_2^2 \int_0^\infty du_3 u_3^2 \mathcal{K}^2(u_2, u_3) + \int_0^\infty dv_2 v_2^2 \int_0^\infty dv_3 v_3^2 \mathcal{H}^2(v_2, v_3) = 1$.

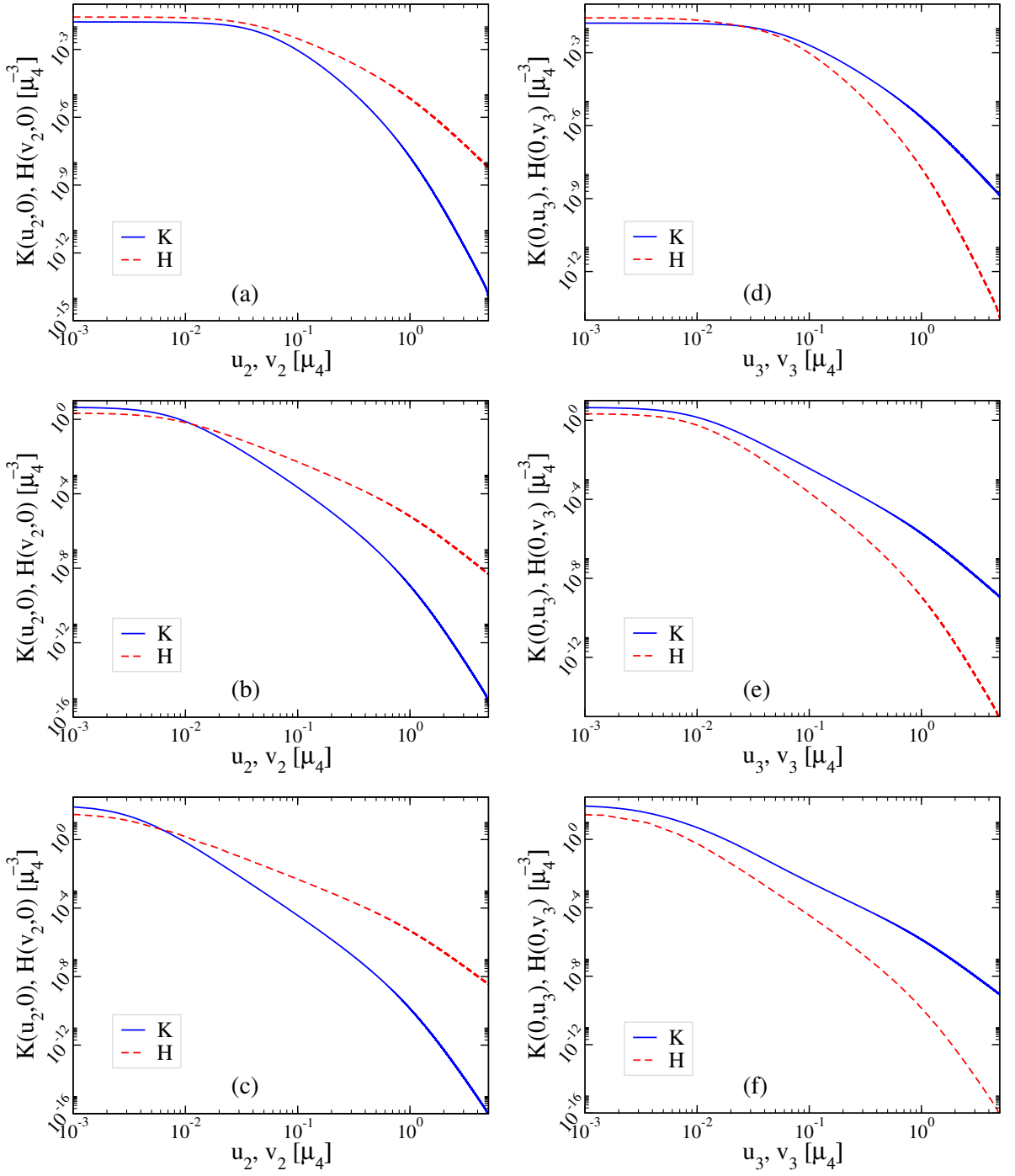


FIG. 7. (Color on-line) Following the caption of Fig. 6, here we have the same quantities for $\mu_4/\mu_3 = 50$. In (a) and (d) we have the ground state; in (b) and (e), the first excited state; and in (c) and (f), the second excited state.

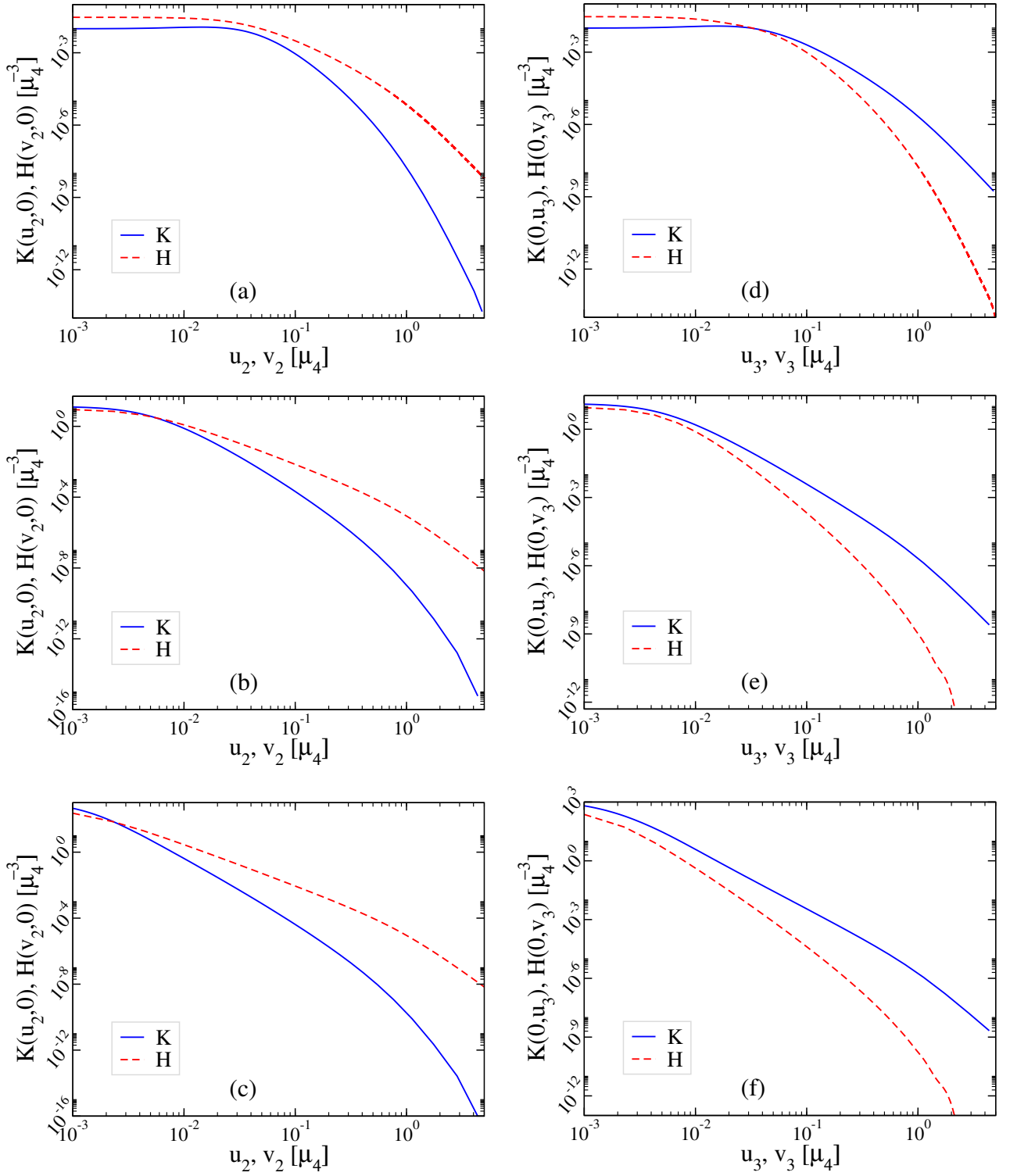


FIG. 8. (Color on-line) Following the caption of Fig. 6, here we have the same quantities for $\mu_4/\mu_3 = 200$. As for $\mu_4/\mu_3 = 50$, here we have another case with two four-body excited states. In (a) and (d) we have the ground state; in (b) and (e), the first excited state; and in (c) and (f), the second excited state.

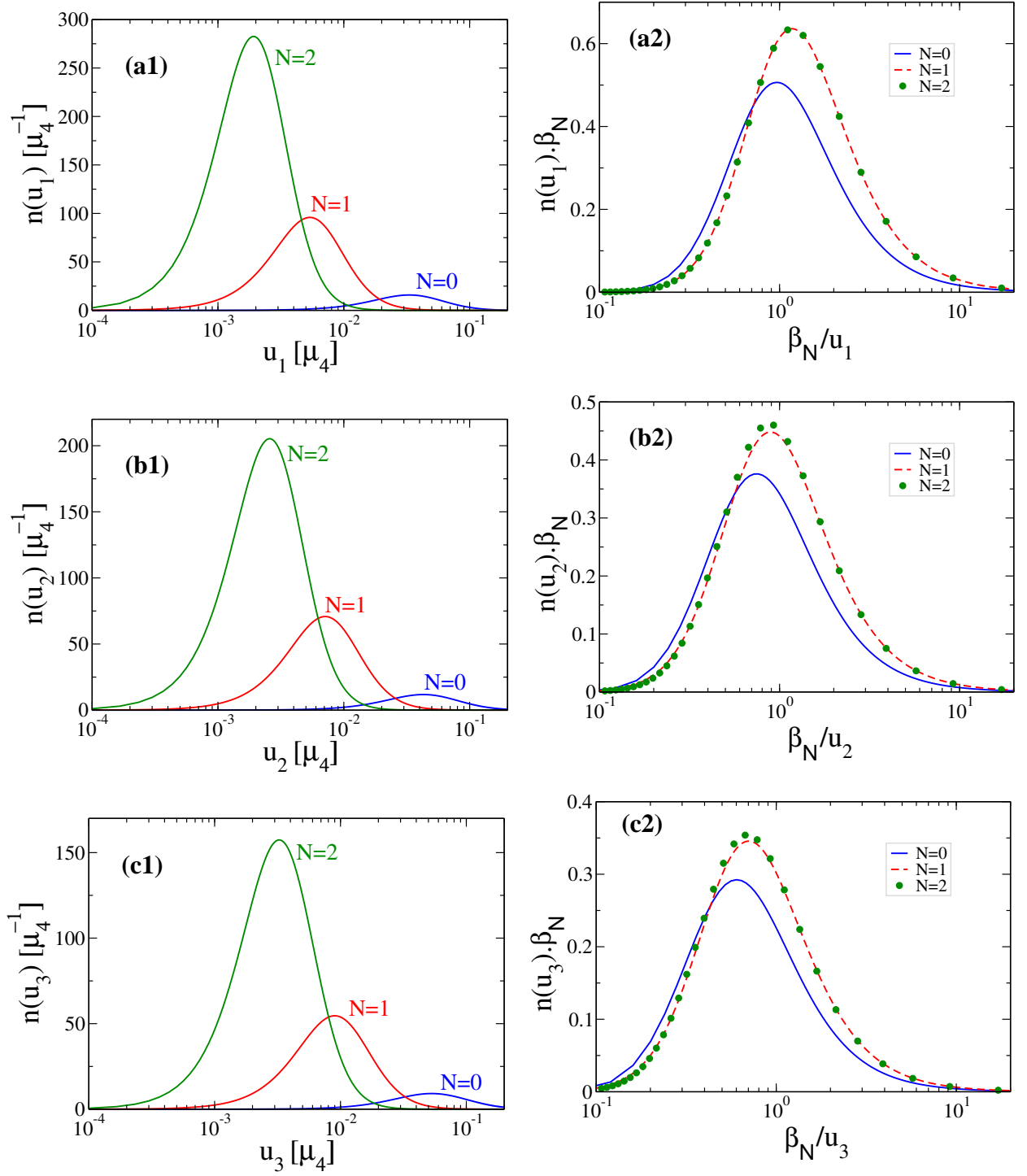


FIG. 9. (Color on-line) Momentum distribution functions $n(u_1)$, $n(u_2)$ and $n(u_3)$, with scale ratio $\mu_4/\mu_3 = 50$, for the ground ($N = 0$) and the first two ($N = 1, 2$) excited tetramer levels, normalized as shown in Eq. 31. In the left panels, they are given as functions of the corresponding momentum, where all momenta are in units of the momentum scale μ_4 . In the right panels, the momentum distributions are rescaled by the momentum factor $\beta_N \equiv \sqrt{B_4^{(N)}}$, where N is the tetramer level.

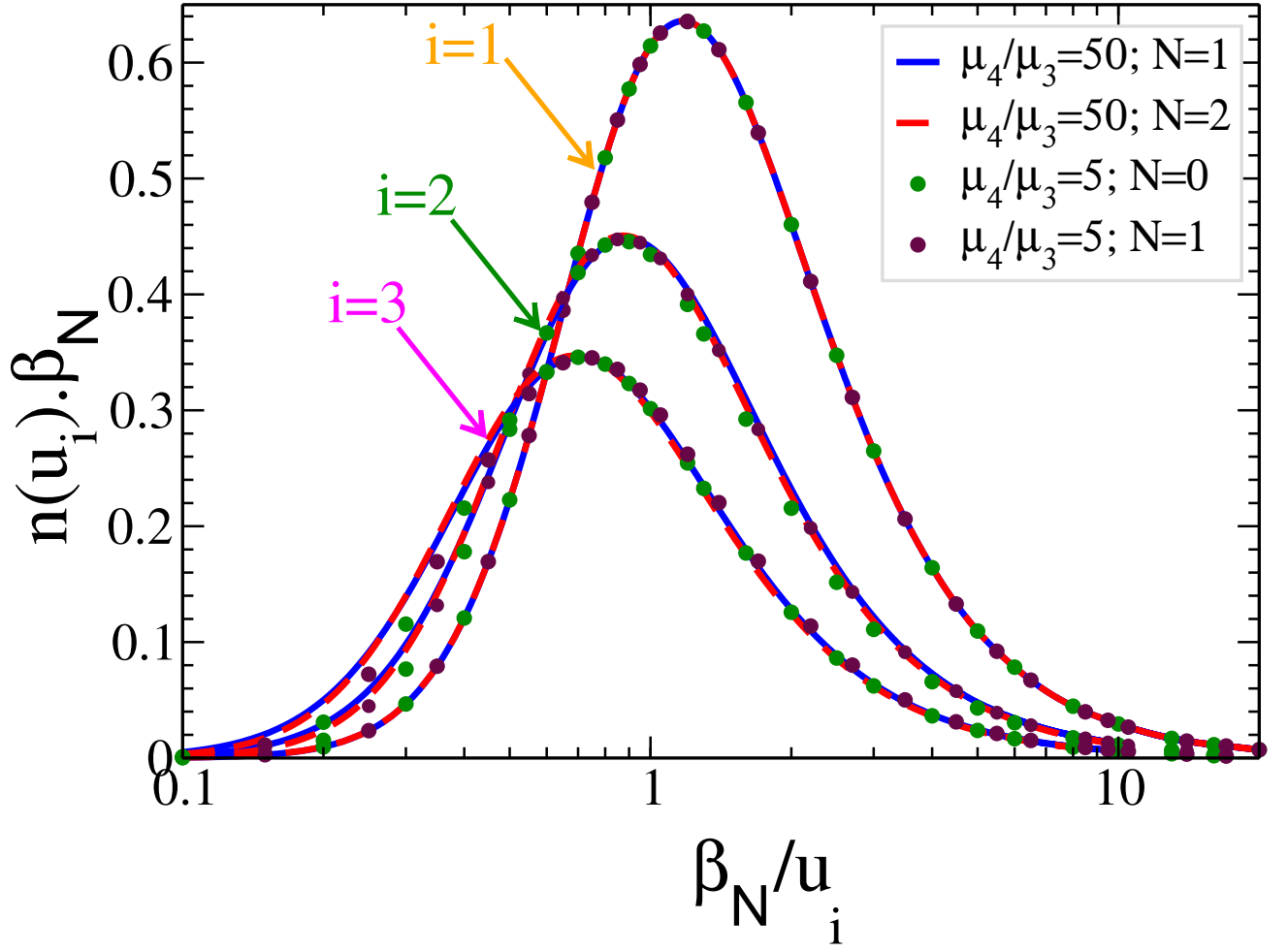


FIG. 10. (Color on-line) Renormalized momentum distributions as functions of the Jacobi momenta $u_{i=1,2,3}$, considering the scaling ratios $\mu_4/\mu_3 = 5$, when there is only one excited state, and $\mu_4/\mu_3 = 50$, when we have two excited states. The units are given by the momentum factor $\beta_N \equiv \sqrt{B_4^{(N)}}$. For each momentum component u_i , the corresponding distributions of both scale ratios, when renormalized to the same maximum value, are shown to reduce almost to the same final form (the labels inside the frame are just to indicate the performed calculations).

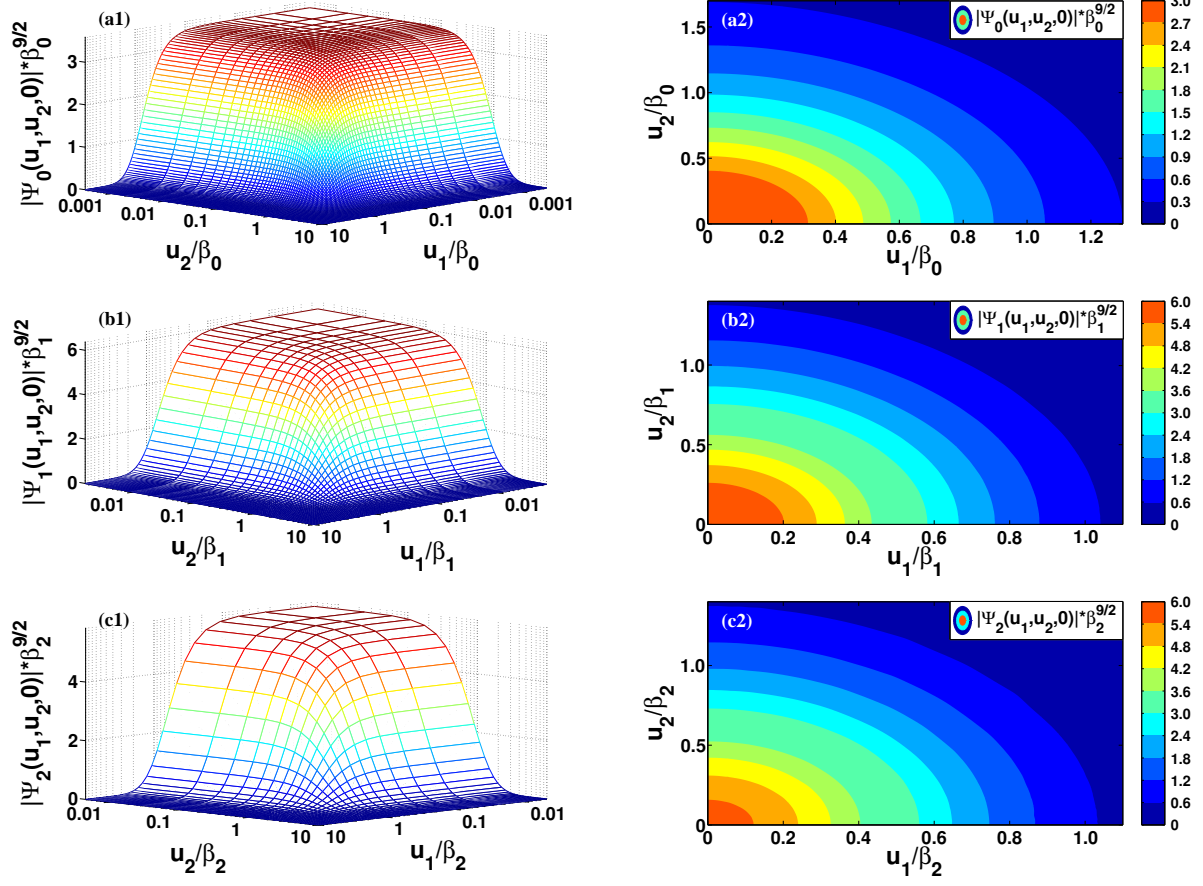


FIG. 11. (Color on-line) The magnitude of the 4B total wave function $\Psi(u_1, u_2, u_3)$ as a function of u_1 and u_2 , with $u_3 = 0$, for the scale ratio $\mu_4/\mu_3 = 50$. The corresponding contour plots are shown for low momentum region, near the peak of the wave function.

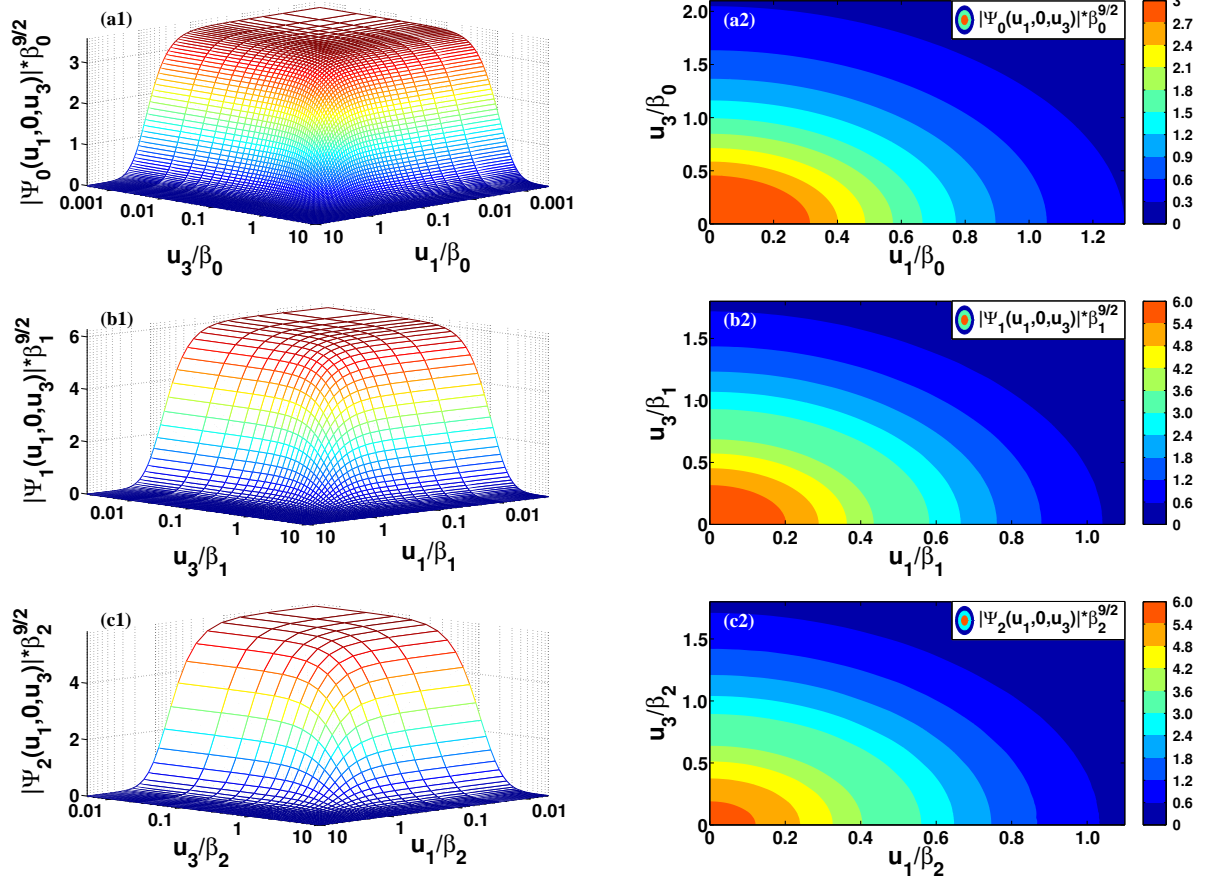


FIG. 12. (Color on-line) As in Fig. 11, the wave-function is given in terms of u_1 and u_3 , with $u_2 = 0$.

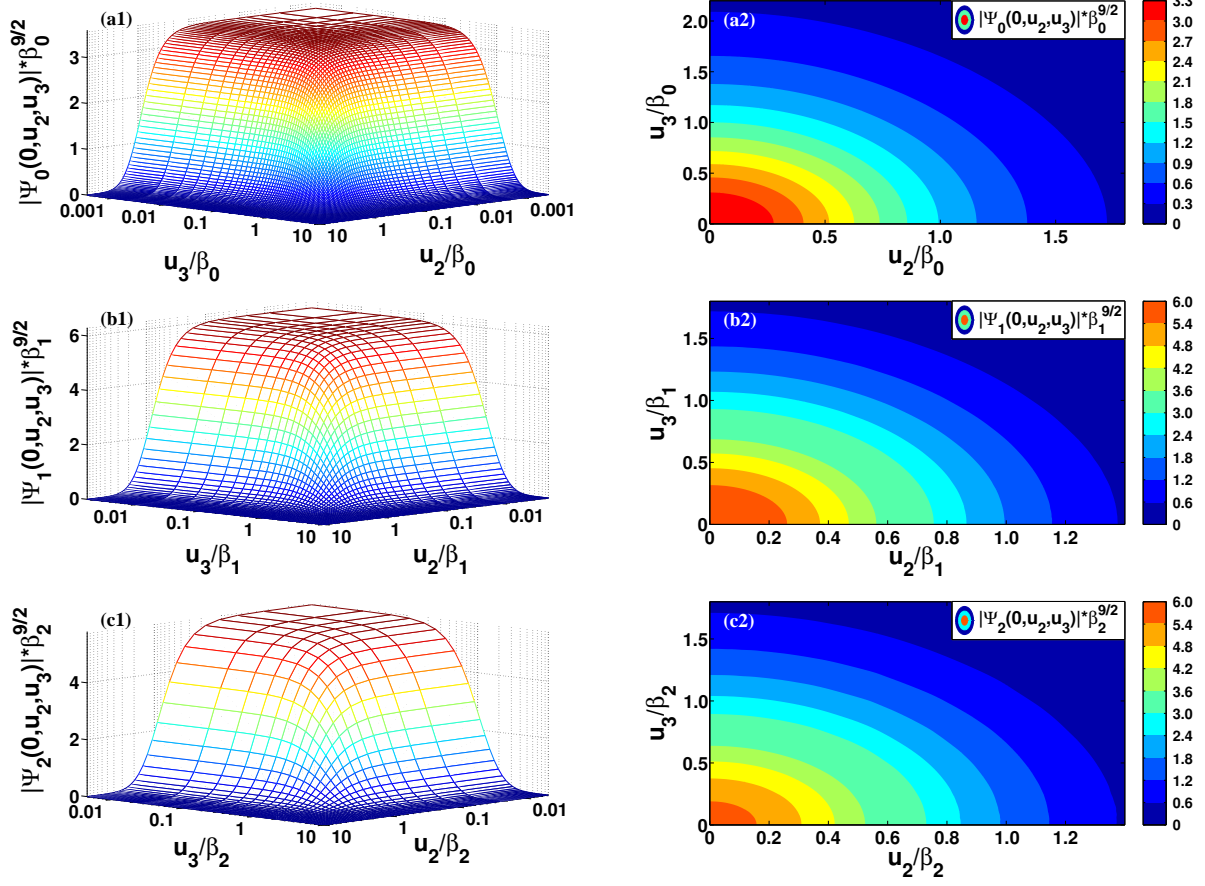


FIG. 13. (Color on-line) As in Fig. 11, the wave-function is given in terms of u_1 and u_3 , with $u_2 = 0$.

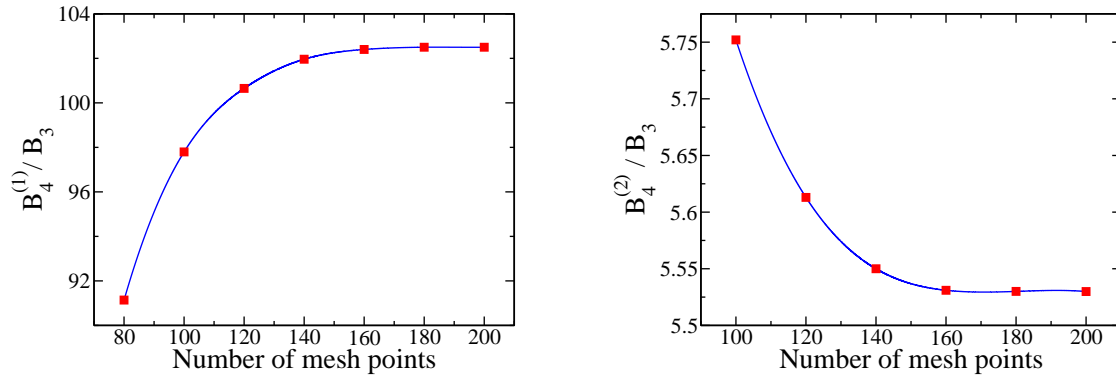


FIG. 14. (Color on-line) Convergence of numerical results for the first and second excited state energies, in the case that $\mu_4/\mu_3 = 300$.